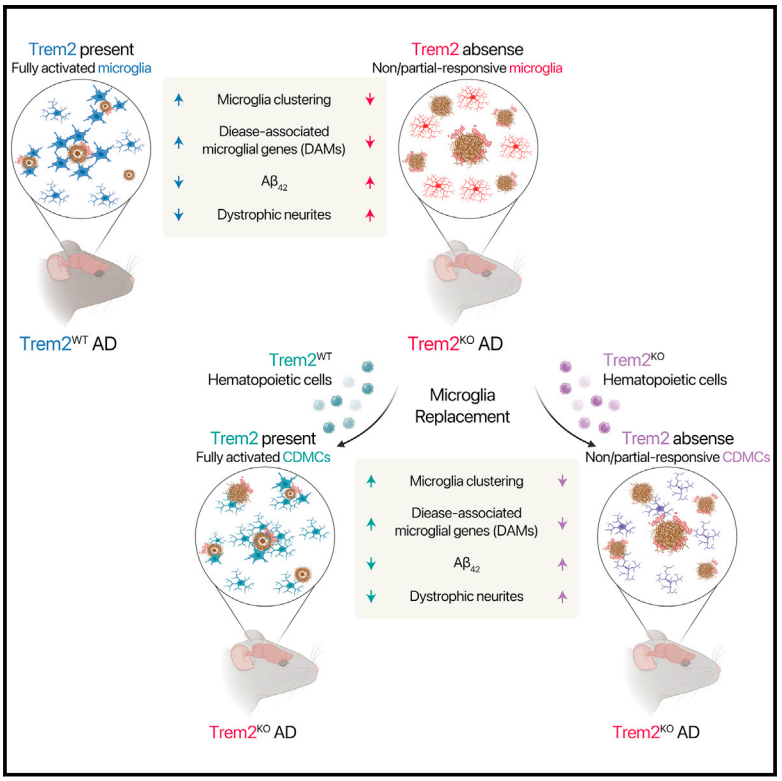
Cell Stem Cell

Article

A cell therapy approach to restore microglial Trem2 function in a mouse model of Alzheimer's disease

Graphical abstract



Authors

Yongjin Yoo, Gernot Neumayer, Yohei Shibuya, Marius Marc-Daniel Mader, Marius Wernig

Correspondence

wernig@stanford.edu

In brief

Mutations of the microglial receptor TREM2 leads to a premature neurodegeneration syndrome, and specific genetic variants are associated with Alzheimer's disease. Yoo et al. show that high-efficiency microglia replacement represents a promising cell therapy to restore Trem2 function in a Trem2-dependent Alzheimer's disease mouse model.

Highlights

- Impaired Trem2 signaling in microglia abolishes their response to Aβ plaques in mice
- Transient CSF1R inhibition enables high-efficiency microglia replacement in 5xFAD mice
- Transplantation of Trem2$^{+/+}$ CDMCs increases reactivity and decreases plaque load
- CDMCs restores DAM gene expression with Syk signaling-dependent transcription

Yoo et al., 2023, Cell Stem Cell *30*, 1043–1053
August 3, 2023 © 2023 Elsevier Inc.
https://doi.org/10.1016/j.stem.2023.07.006

CellPress

Cell Stem Cell

CellPress

Article

A cell therapy approach to restore microglial Trem2 function in a mouse model of Alzheimer's disease

Yongjin Yoo,[1] Gernot Neumayer,[1] Yohei Shibuya,[1] Marius Marc-Daniel Mader,[1] and Marius Wernig[1,2,3,*]
[1]Institute for Stem Cell Biology and Regenerative Medicine and Department of Pathology, Stanford University School of Medicine, Stanford, CA 94305, USA
[2]Department of Chemical and Systems Biology, Stanford University School of Medicine, Stanford, CA 94305, USA
[3]Lead contact
*Correspondence: wernig@stanford.edu
https://doi.org/10.1016/j.stem.2023.07.006

SUMMARY

Alzheimer's disease (AD) remains one of the grand challenges facing human society. Much controversy exists around the complex and multifaceted pathogenesis of this prevalent disease. Given strong human genetic evidence, there is little doubt, however, that microglia play an important role in preventing degeneration of neurons. For example, loss of function of the microglial gene Trem2 renders microglia dysfunctional and causes an early-onset neurodegenerative syndrome, and Trem2 variants are among the strongest genetic risk factors for AD. Thus, restoring microglial function represents a rational therapeutic approach. Here, we show that systemic hematopoietic cell transplantation followed by enhancement of microglia replacement restores microglial function in a Trem2 mutant mouse model of AD.

INTRODUCTION

The pathogenesis of Alzheimer's disease (AD) is complex and not well understood.[1] Familial forms of the disease are caused by mutations affecting the proteolytic processing of Alzheimer precursor protein (APP), resulting in overproduction of the APP cleavage product amyloid beta (Aβ), which is the main component of senile plaques, a diagnostic criterion of AD.[1,2] Despite the poor correlation between the presence of senile plaques and clinical presentation, the Aβ hypothesis is the basis of most therapeutic strategies currently being pursued and remains controversial.[3,4] On the other hand, genome-wide association studies (GWASs) in sporadic, late-onset AD have identified many variants in microglial genes enriched in patients, including the variant *TREM2*^{R47H}, which is among the strongest genetic risk factors for the disease.[5–7] Accordingly, genetic loss of function of *TREM2* results in Nasu-Hakola disease, a rare syndrome characterized by an early-onset neurodegeneration of frontotemporal dementia associated with cyst-like bone lesions.[8–10] These data convincingly demonstrate that dysfunctional microglia can cause neurodegeneration, and one of the normal functions of microglia is to prevent neurodegeneration in the healthy brain. Thus, restoring the function of mutant microglia and enhancing normal microglial function represent a promising therapeutic strategy based on a solid scientific foundation. In this paper, we explored whether Trem2 function can be restored by replacing mutant microglia throughout the brain with circulation-derived myeloid cells (CDMCs) following hematopoietic cell transplantation in a mouse model of AD.

RESULTS

Transplanted, bone-marrow-derived CDMCs efficiently replace microglia in 5xFAD brains and react to Aβ plaques

First, we sought to investigate the effects of replacing brain-resident microglia with CDMCs in a mouse model of AD. In order to permanently label donor bone marrow cells, we crossed 5xFAD mice, an aggressive mouse model of AD that develops Aβ pathology beginning at 1.5 months of age,[11,12] with Ubc-GFP mice to obtain 5xFAD; GFP mice.[13] Using bone marrow cells from these mice as donor cells, we then performed high-efficiency microglia replacement by bone marrow transplantation (mrBMT) enabled by a transient treatment with the CSF1R inhibitor PLX5622 in 3-week-old 5xFAD mice (Figures 1A and 1B) developed by us and others.[14,15] Flow cytometry and histology demonstrated efficient (>90%) and sustained hematopoietic cell chimerism of grafted cells in peripheral blood and brain for at least 5 months (Figures 1C and 1D). In BMT-only control mice, the chimerism in the blood was >90%, but in the brain, it was variable and averaging around 20%. Histological examination revealed a homogeneous, widespread incorporation of GFP$^+$ cells (Figure 1E), displaying a ramified morphology and immunoreactivity for Iba-1 (Figures 1F and 1G).

Microglia are known to restrict the spread of Aβ by tightly wrapping around plaques to form a physical barrier to restrain the outward extension of amyloid fibrils and promote formation

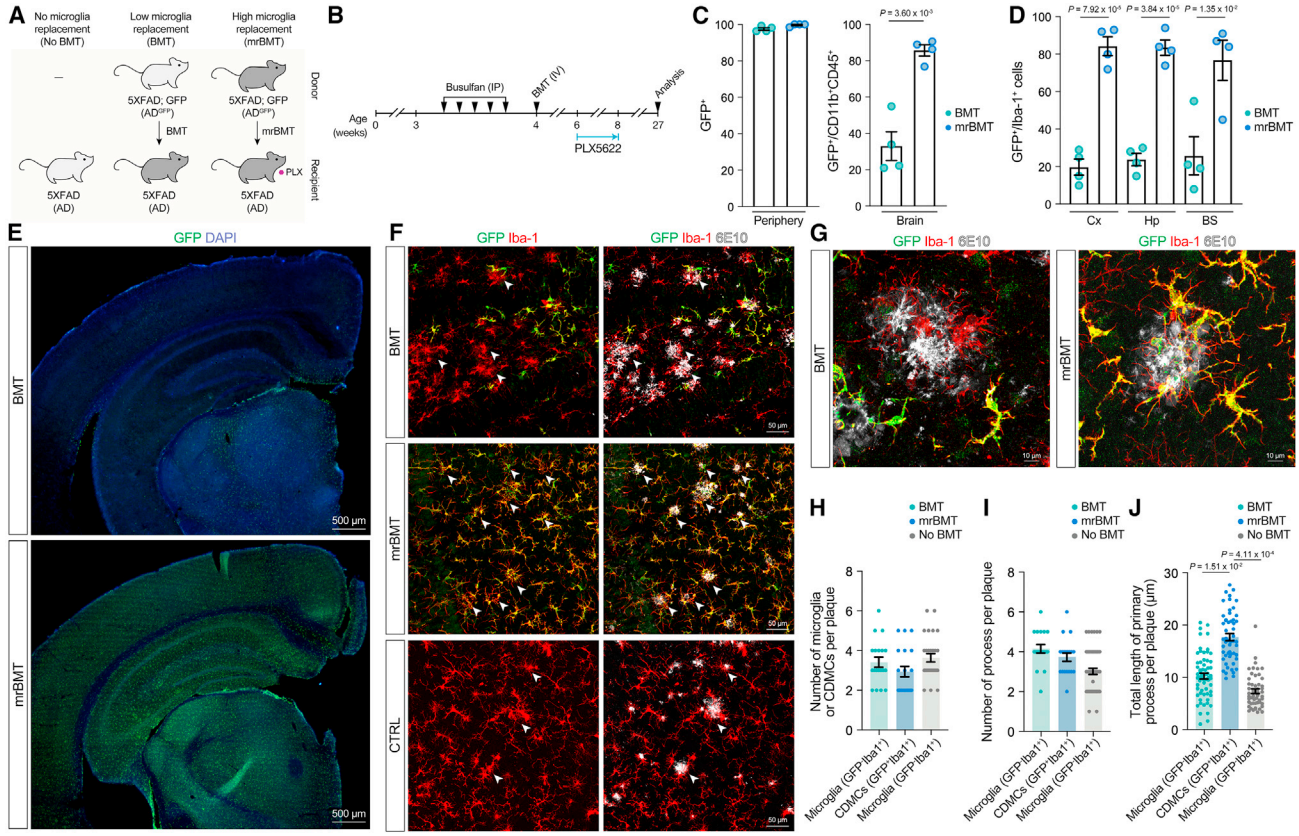


Figure 1. Brain-incorporated CDMCs react to Aβ plaques similar to microglia

(A and B) Schematic overview of BMT followed by PLX5622 treatment in 5xFAD mice.

(C) Myeloid chimerism in the peripheral blood and brain was analyzed by flow cytometry. Each data point represents one mouse of hemi brain, n = 4 mice per group.

(D) Quantification of GFP$^+$ (green) Iba-1$^+$ (red) cells in the cortex (Cx), hippocampus (Hp), and brain stem (BS). Data points represent the average of n = 4 per group, three brain slices per animal.

(E) Representative coronal brain sections showing GFP$^+$ CDMCs and DAPI.

(F and G) Representative confocal images of GFP$^+$Iba-1$^+$ cells with Aβ (6E10, gray) staining in the cortex. Arrowheads indicate plaque-associated microglia or CDMCs.

(H) The number of microglia (GFP$^-$Iba-1$^+$) or CDMCs (GFP$^+$Iba-1$^+$) within 15 µm of 6E10$^+$ Aβ plaques. Data point is from representative 19–20 plaques from n = 4 mice per group.

(I and J) Quantification of primary processes and length of primary processes of plaque-associated microglia (GFP$^-$Iba-1$^+$) or CDMCs (GFP$^+$Iba-1$^+$). Data points are from representative 54–64 plaques from n = 4 mice per group.

Statistical significance between experimental groups was calculated by two-tailed unpaired Student's t test. Data are presented as mean ± SEM. Exact p values were indicated.

of highly compact plaques.[16,17] Importantly, transplanted GFP$^+$ CDMCs also clustered around Aβ plaques similar to endogenous microglia (GFP$^-$Iba-1$^+$ cells) in 6-month-old mice (Figures 1F and 1G). The number of myeloid cells per plaque was similar between microglia and CDMCs (Figure 1H). While endogenous microglia often display an activated "ameboid" morphology with shorter processes and larger cell bodies (Figures 1G, 1I, and 1J),[18] we observed that CDMCs were morphologically distinct from microglia with longer primary processes but a comparable number of primary processes per plaque (Figure 1J). Despite this morphological difference of CDMCs, there were no changes in total Aβ loads (Figures S1A and S1B), suggesting that, overall, CDMCs respond to Aβ pathology similarly to microglia in this AD mouse model.[19,20]

Microglia replacement restores microglial activation in *Trem2*$^{-/-}$ 5xFAD mice

Trem2 is known to be necessary for many reactive changes induced by Aβ pathology.[17,21–28] We confirmed the absence of disease-associated microglial (DAM) gene[24,26,28] induction and a relative increase of homeostatic markers (Figures S2A–S2C) as well as a lack of microgliosis as indicated by the lack of Iba-1 and CD45 induction (Figures S2D–S2F and S3C–S3E). We asked whether cell transplantation with Trem2$^{+/+}$ CDMCs may restore this important microglial reaction. To that end, we transplanted bone marrow from either female Trem2$^{+/+}$; 5xFAD; Ubc-GFP (T2WT-AD^{GFP}) or male Trem2$^{+/+}$; 5xFAD (T2WT-AD) mice into female Trem2$^{-/-}$; 5xFAD (T2KO-AD) mice at 3 weeks of age (Figure 2A) or 8 weeks of age (Figure S4). To

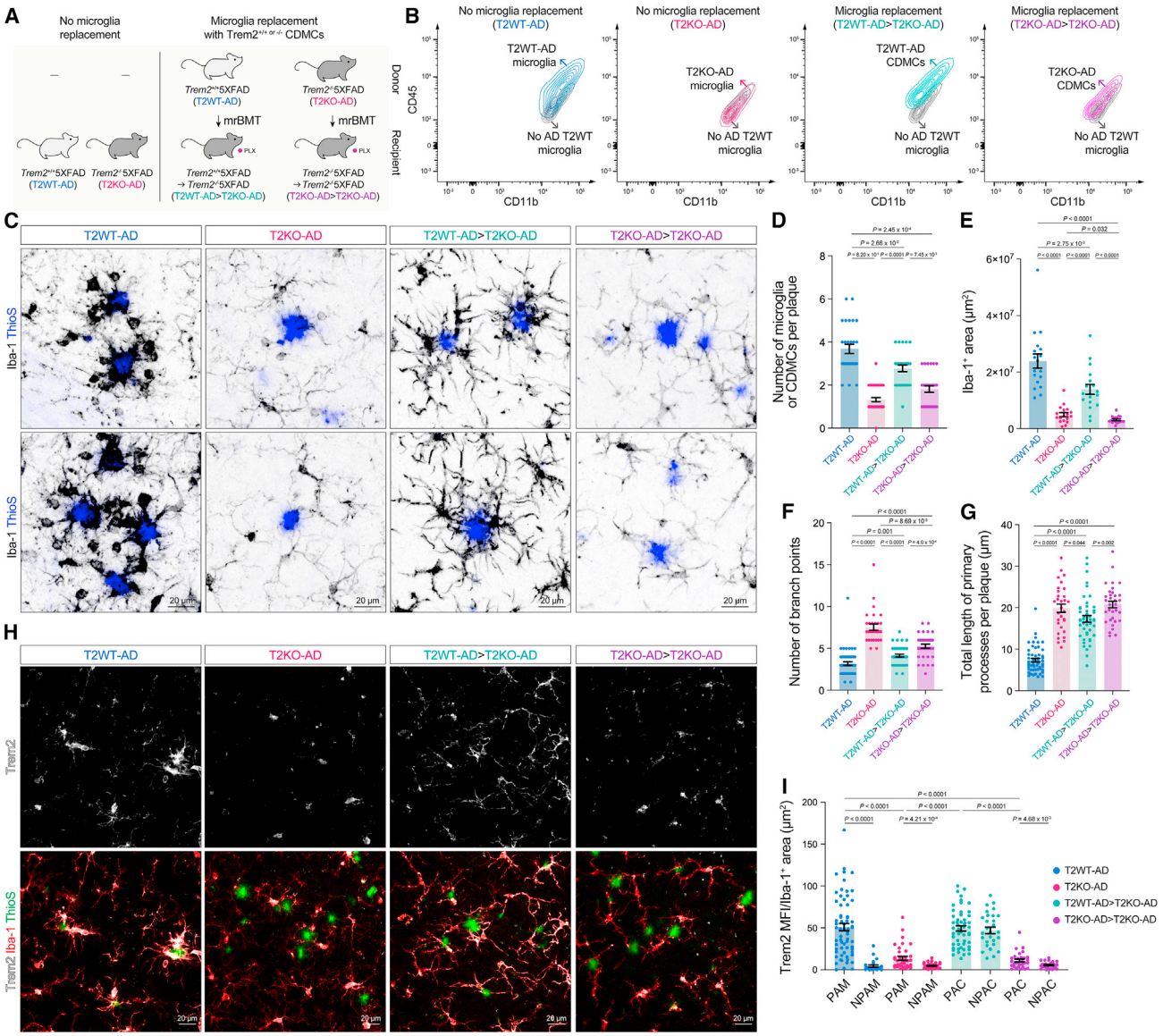


Figure 2. Microglia replacement restores microglial activation in *Trem2*$^{-/-}$ 5xFAD mice

(A) To assess the effect of microglia replacement, we compared T2WT-AD with T2KO-AD mice with T2KO-AD recipient mice transplanted with either therapeutic T2WT-AD cells or negative control T2KO-AD cells. Mice were transplanted at 3 (this figure) or 8 weeks of age (Figure S4) and analyzed at 27 weeks of age.

(B) Microglia show a characteristic upregulation of CD45 in 5xFAD mice as determined by flow cytometry (compare gray with blue signal). CD45 upregulation is Trem2 dependent (compare gray with red signal). The CD45 upregulation is restored upon therapeutic CDMC transplantation (compare gray with cyan signal). Trem2$^{-/-}$ CDMCs could not rescue the CD45 activation phenotype (compare gray with magenta signal). The gray signal, "no AD T2WT microglia," was obtained from age-matched (27 weeks), normal, female C57B6 mice. Replicates and quantifications are shown in Figure S3.

(C) Projected confocal images of Iba-1^{+} microglia (black) and Thioflavin S (ThioS)-labeled Aβ plaques (blue) show a clear rescue of microglia activation by Aβ plaques following Trem2$^{+/+}$ cell transplantation.

(D and E) The number and quantification of the Iba-1 immunofluorescence area of microglia or CDMCs within a 15 μm radius around ThioS-labeled plaques. Data points are from representative 19–30 plaques from n = 4–5 mice per group.

(F and G) The number of branch points per Iba-1^{+} cell and total length of primary processes of plaque-associated Iba-1^{+} cells. Data points are from representative 31–51 plaques from n = 4–5 mice per group.

(H) Restoration of plaque-enriched Trem2 expression after CDMC transplantation as shown by confocal immunofluorescence microscopy of Iba-1^{+} (red), Trem2^{+} (gray), and ThioS-labeled Aβ plaques (green) in the cortex.

(I) Quantification of Trem2 mean fluorescence intensity (MFI) in cortical Iba-1^{+} cells. Plaque-associated microglia (PAM) and non-plaque-associated microglia (NPAM), as well as plaque-associated CDMCs (PAC) and non-plaque-associated CDMCs (NPAC), were counted separately. Data points are from representative 59–103 plaques from n = 4–5 mice per group.

Statistical significance between experimental groups was calculated by two-tailed unpaired Student's t test. Data are presented as mean ± SEM. Exact p values were indicated.

control for the effects of the mrBMT procedure itself, we also transplanted T2KO-AD cells into T2KO-AD recipients. Flow cytometry and droplet digital PCR confirmed a high chimerism of GFP$^+$ or Y chromosome$^+$ donor cells, respectively (Figures S3A, S3B, and S4A). First, we assessed CD45 and CD11b expression by flow cytometry. As observed in normal mice,[14,15] mutant CDMCs already showed a slight overexpression of these markers (Figures 2B and S3C–S3E). Transplantation of T2WT-AD donor cells, on the other hand, resulted in an almost complete restoration of CD45 and CD11b expression (Figures 2B and S3C–S3E). To assess microglial morphology, we next performed immunohistochemistry. Iba-1 staining illustrated an increased activation of transplanted Trem2$^{+/+}$ CDMCs around Aβ plaques, akin to the microglia reaction in normal 5xFAD mice but unlike in brains transplanted with Trem2$^{-/-}$ CDMCs (Figure 2C). The number of Iba-1$^+$ myeloid cells was rescued well but not completely (Figure 2D), and morphometric analyses of myeloid cells showed obvious partial rescues, such as Iba-1 immunofluorescence intensity, number of branch points, and primary process length (Figures 2E–2G). While no statistically significant difference was observed among non-plaque-associated Iba-1$^+$ microglial cells between T2WT-AD and T2KO-AD, which is consistent with a previous study,[26] cell density was slightly increased in the brains transplanted with Trem2$^{+/+}$ CDMCs (Figures S4B and S4C). Finally, we assessed the rescue of Trem2 expression itself, which is known to be primarily induced in Aβ plaque-associated microglia.[25] Reassuringly, we found a robust upregulation of Trem2 in transplanted CDMCs—in particular, in plaque-associated CDMCs (Figures 2H and 2I). Of note, we also found an increase of Trem2 in non-plaque-associated CDMCs, albeit at lower levels.

Transplanted Trem2$^{+/+}$ CDMCs reduce Aβ deposition and LAMP1$^+$ dystrophic neurites, induce Aβ plaque compaction, and restore Aβ plaque phagocytosis

Having observed restoration of microglial activity, we next asked whether microglia replacement therapy would also have an impact on Aβ pathology. Indeed, immunofluorescence labeling of Aβ using the well-described antibody 6E10 demonstrated a clear reduction of overall Aβ load following replacement of Trem2$^{-/-}$ microglia with Trem2$^{+/+}$ CDMCs, almost down to the level of 5xFAD mice with intact Trem2 when transplanted at 3 weeks of age (Figures 3A and 3B). The effects were similar but less pronounced when cells were transplanted at 8 weeks of age (Figures S4D and S4E), suggesting that Trem2$^{+/+}$ cells may primarily prevent formation of new plaques rather than dissolving existing plaques consistent with previous findings.[12] As loss of Trem2 function is known to affect plaque shape,[26,27,29] we quantified the Aβ plaque circularity and area in the four different conditions. Again, Trem2$^{+/+}$ CDMC transplantation resulted in more compacted Aβ plaques, as also illustrated by the morphometric analysis (Figures 3C–3E). Trem2-deficient microglia are known to have a deficiency in Aβ material internalization.[30] 3D reconstructions of phagosome marker CD68,[31] myeloid cell marker Iba-1, and Thioflavin S demonstrated that Trem2$^{+/+}$ CDMCs had increased phagosomes, which contained Aβ material unlike that in T2KO-AD brains (Figures 3F–3H). In addition to modulating Aβ pathology, Trem2 deficiency also leads to higher levels of axonal dystrophy in mouse AD models.[17,29,32–34] Lamp1, a selective marker of late endosomes and lysosomes, has been used to label vesicles accumulating in dystrophic neurites.[16,35] The increase of total Lamp1 volume around 6E10-labeled Aβ plaques in Trem2-mutant mice was almost completely rescued following transplantation with Trem2$^{+/+}$ CDMCs (Figures 3I and 3J).

The DAM transcriptional program is restored following microglia replacement with *Trem2*$^{+/+}$ CDMCs

Microglia are known to induce a characteristic transcriptional program in neurodegenerative disease, the so-called DAM program.[28] The DAM state is partially Trem2 dependent and thought to endow microglia with important neuroprotective machinery. Therefore, we next used RNA sequencing (RNA-seq) to elucidate whether Trem2$^{+/+}$ CDMCs re-installed DAM gene acquisition in T2KO-AD brains (Figure 4). CD11b$^+$CD45$^+$ microglia from T2WT-AD, T2KO-AD, and non-transgenic naive (No-AD T2WT) mice and GFP$^+$/CD11b$^+$CD45$^+$ CDMCs from T2WT-AD > T2KO-AD and T2KO-AD > T2KO-AD mice were fluorescence-activated cell sorting (FACS) isolated, and whole transcriptomes were generated for RNA-seq analysis (Figure 4A). Indeed, *Trem2*, as well as stage II DAM gene expression, was significantly restored in Trem2$^{+/+}$ CDMCs compared to Trem2$^{-/-}$ microglia and Trem2$^{-/-}$ CDMCs (Figures 4B and 4I). Overall, we observed 872 upregulated and 1,259 downregulated genes with a cutoff of log2 fold change ±1 and $p_{adj.} < 0.05$ when comparing Trem2$^{+/+}$ CDMCs and Trem2$^{-/-}$ microglia (Figures 4B and S5B; Table S3). Gene ontology (GO) and pathway analysis showed that Trem2$^{+/+}$ CDMCs had elevated expression of genes involved in lipid storage and MAPK signaling pathways (Figures 4C and S5A; Table S3). Of note, MAPK signaling and lipid pathways were previously found to be suppressed in TREM2-knockout-induced pluripotent stem cell-derived human microglia[36] and in Trem2-deficient mice.[37]

We then performed enrichment analysis of differentially expressed genes with well-characterized microglial gene sets (Figures 4D and S5C; Table S3).[28,38–40] Consistent with previous studies,[28,41] we observed downregulation of stage II DAM- and Aβ plaque phagocytosis-associated genes upon Trem2 deletion (Figure 4D). These signatures were significantly restored in transplanted Trem2$^{+/+}$ CDMCs, but not in Trem2$^{-/-}$ CDMCs (Figures 4D–4F). For example, the DAM genes *Axl*, *Itgax*, and *Lpl* were increased Trem2$^{+/+}$ CDMCs (Figures 4F and S5D). Moreover, the 14 most authentically restored genes were also enriched in stage II DAM genes ($p_{adj.} = 3.31 \times 10^{-9}$, 78.6%) (Figures 4G–4I) and downregulated in microglial cells of Trem2$^{-/-}$ 5xFAD mice (Figures S5E and S5F; Table S3).[41] We also confirmed that the expression patterns of these genes were increased in human AD patients with high National Institute on Aging-Reagan scores (Figure S5G),[42] suggesting that these genes may play an important role in the regulation of Trem2-associated microglia activation in amyloid pathology.

Restoration of Syk signaling-dependent genes, as well as the microglial surface receptors Clec7a and CD11c, following *Trem2*$^{+/+}$ CDMC transplantation

Syk is a key downstream signaling factor enabling measurable activation of the Trem2 receptor, as well as other cell surface signaling receptors such as C-type lectin domain family 7

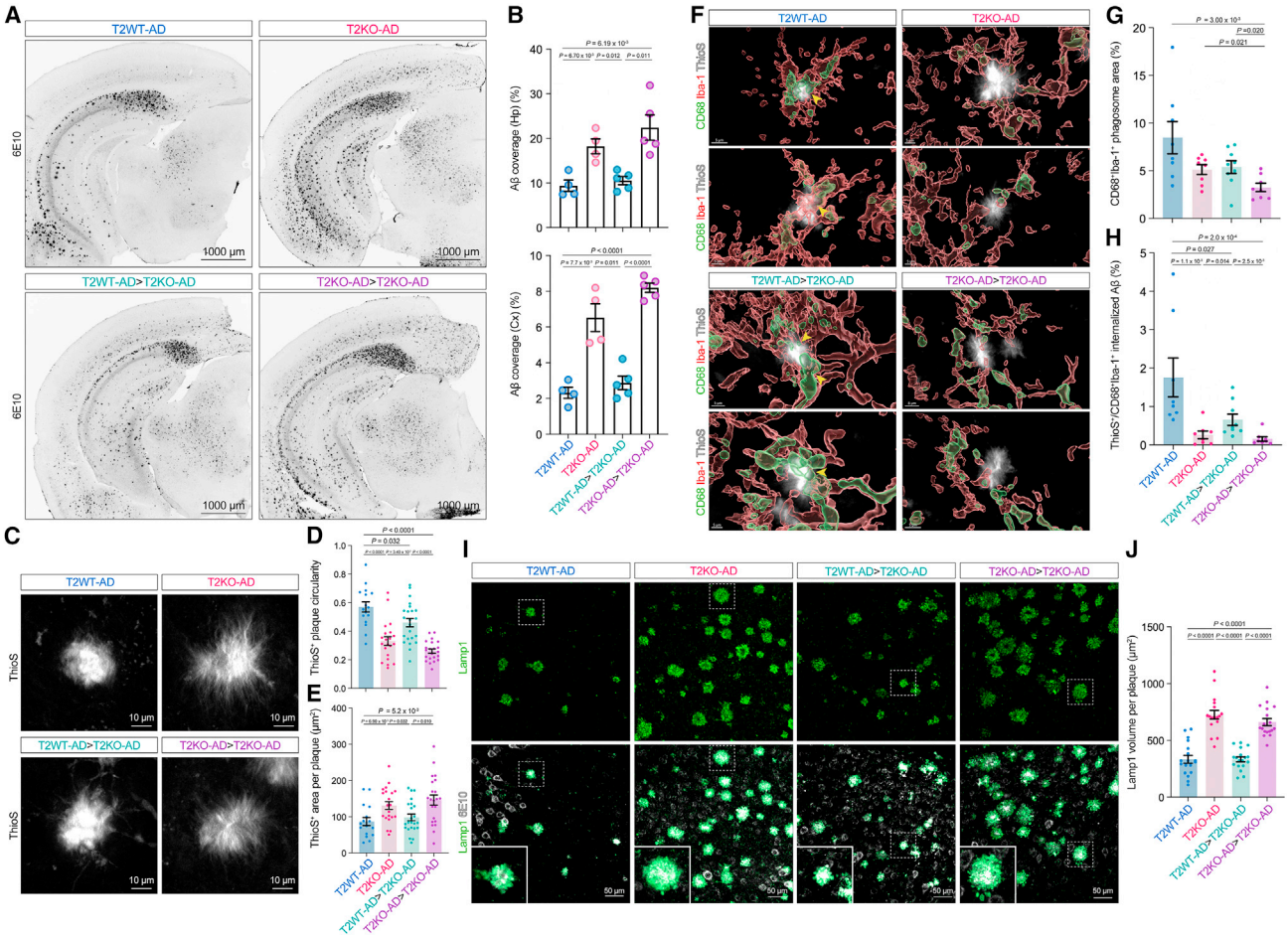


Figure 3. Transplanted Trem2$^{+/+}$ CDMCs reduce Aβ deposition, induce Aβ plaque compaction, restore Aβ plaque phagocytosis, and reduce LAMP1^{+} dystrophic neurites

(A) Representative immunofluorescence staining of 6E10-labeled Aβ (black) on coronal sections of mice with the four indicated conditions at 27 weeks of age.

(B) Quantification of 6E10-covered area in cortex (Cx) and hippocampus (Hp). Each data point represents an individual mouse. n = 4–5 mice per group.

(C) Representative confocal images of Thioflavin S (ThioS)-labeled Aβ plaques (gray) in the cortex of mice from the four indicated conditions. Note the diffuse (in T2KO-AD, T2KO-AD > T2KO-AD) and compact (in T2WT-AD, T2WT-AD > T2KO-AD) plaques.

(D and E) Quantification of ThioS^{+} Aβ plaque circularity and ThioS-covered area. Data points are from representative 96–132 plaques from n = 4–5 mice per group.

(F) 3D reconstructions of CD68^{+} (green) endosomal/lysosomal compartment and Iba1^{+} cells (red) with ThioS-labeled Aβ (gray) show rescue of phagocytosis activity upon Trem2$^{+/+}$ CDMCs transplantation. Arrowheads indicate phagosome area (CD68^{+}ThioS^{+}) within Iba-1^{+} area.

(G and H) Quantification of phagosome activity (CD68^{+}/Iba-1^{+} within 15 μm from ThioS^{+} plaque) and internalized Aβ within CD68^{+}Iba-1^{+} area. Data points represent the average of n = 4–5 per group, three brain slices per animal.

(I) Representative confocal images of 6E10-labeled Aβ plaques (gray) and Lamp1^{+} dystrophic neurites (green) in the four conditions indicated. Insets: higher magnification of dystrophic neurites indicated by dashed line boxes.

(J) Quantification of Lamp1^{+} dystrophic neurites volume per plaque. Data points are from representative 18–21 ThioS^{+} plaques from n = 4–6 mice per group.

Statistical significance between experimental groups was calculated by two-tailed unpaired Student's t test. Data are presented as mean ± SEM. Exact p values were indicated.

member A (Clec7a), CD11c, and CD33.[28,43–48] Recent studies have shown that Syk-deficient AD model mice induced fewer DAM genes, increased plaques, and worsened memory function.[49,50] Moreover, microglia lacking Syk have lower phosphorylated AKT levels and reduced expression of genes involved in glycolysis and mTORC1 signaling (Figure 5A).[50] Therefore, we evaluated whether the expression of genes repressed in Syk-deficient 5xFAD microglia was restored in Trem2$^{+/+}$ CDMCs. We observed that 12 out of 31 Syk-dependent genes ($p_{adj.}$ < 0.05, 38.7%) were also downregulated in Trem2$^{-/-}$ microglia of our current RNA-seq analysis, and 9 out 12 genes were significantly elevated in Trem2$^{+/+}$ CDMCs (Figures 5B and 5C; Table S3). In addition, the expression of the lipoprotein lipase (Lpl) gene, which is known to be significantly reduced in 5xFAD Syk$^{\Delta MG}$ microglia,[49] was significantly increased in Trem2$^{+/+}$ CDMCs, suggesting that Lpl-mediated lipid homeostasis and lipid droplet formation may have been restored in Trem2$^{+/+}$ CDMCs.[51,52]

Clec7a is known to be induced in DAMs during neurodegeneration[54,55] and also signals through Syk tyrosine kinase.[56]

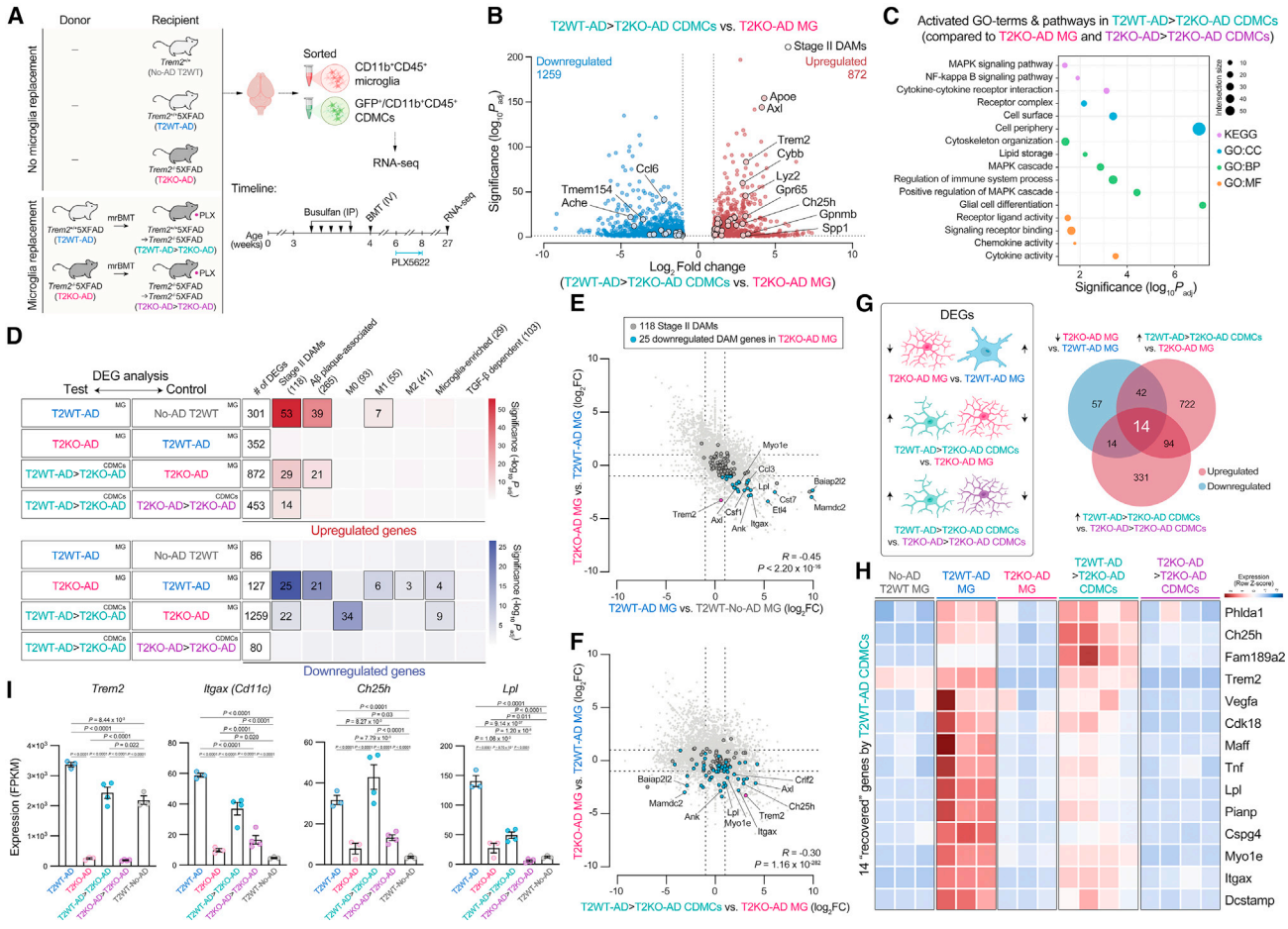


Figure 4. Microglia replacement with Trem2$^{+/+}$ CDMCs restores attenuated disease-associated microglia transcriptional program of Trem2$^{-/-}$ 5xFAD brain

(A) Schematic of experimental design for RNA-seq analysis.

(B) Volcano plot presenting significantly upregulated (red) and downregulated (blue) (cutoff of Log2 fold change ±1; $p_{adj} < 0.05$) genes in Trem2$^{+/+}$ CDMCs compared to Trem2$^{-/-}$ microglia. Dot with black circle highlights known stage II disease-associated microglial (DAM) genes.

(C) Gene ontology (GO) terms and pathway enrichment scatterplot highlighting major pathways that are activated in Trem2$^{+/+}$ CDMCs compared to Trem2$^{-/-}$ microglia and Trem2$^{-/-}$ CDMCs.

(D) Heatmap showing overlapping significance of differentially expressed genes with known microglia gene sets.[28,38–40] Significantly overlapped gene sets ($p_{adj.} < 0.05$) are highlighted with black boxes and the exact number of overlapping genes.

(E and F) Correlation of changes in gene expression between Trem2$^{+/+}$ microglia and Trem2$^{-/-}$ microglia (y axis) and between Trem2$^{+/+}$ microglia and No-AD Trem2$^{+/+}$ microglia (x axis) (E) and between Trem2$^{+/+}$ microglia and Trem2$^{-/-}$ microglia (y axis) and between Trem2$^{+/+}$ CDMCs and Trem2$^{-/-}$ microglia (x axis) (F). Darker gray dots highlight stage II DAM genes. Dots with cyan color highlights significantly downregulated DAMs in Trem2$^{-/-}$ microglia. *R*, correlation coefficient; *P*, p value for linear regression analysis.

(G) Schematic diagram for identification of key genes recovered from Trem2$^{+/+}$ CDMCs. Venn diagram showing the number of downregulated genes (blue) in Trem2$^{-/-}$ microglia compared to Trem2$^{+/+}$ microglia and upregulated genes (red) in Trem2$^{+/+}$ CDMCs compared to Trem2$^{-/-}$ microglia and Trem2$^{-/-}$ CDMCs.

(H) Heatmap representation of significantly recovered genes in Trem2$^{+/+}$ CDMCs with Trem2$^{-/-}$ microglia or Trem2$^{-/-}$ CDMCs.

(I) Read counts (FPKM) from RNA-seq differentially expressed genes for *Trem2*, *Itgax*, *Ch25h*, and *Lpl*.

Statistical significance between groups was calculated by Wald test of DESeq2 package (B and I) and hypergeometric test for gene overlap testing (D). Data are presented as mean ± SEM. Exact p values were indicated. MG, microglia; DEG, differentially expressed genes.

Furthermore, *Trem2*^{R47H}; 5xFAD mice injected with Clec7a-activating antibodies displayed less filamentous plaques and compacted Aβ plaques, indicating that microglial Clec7a activation can boost Aβ clearance (Figure 5D).[49,50] Notably, Cd11c, another microglial surface receptor signaling via Syk and itself downstream of Clec7a signaling, fails to be induced in Trem2$^{-/-}$ mice, and its expression is restored in Trem2$^{+/+}$ CDMCs (Figures 4H and 4I). Moreover, its expression positively correlates with Trem2 expression (Figure 5E). Immunofluorescence and qPCR analyses corroborated increased expression of Clec7a and CD11c in Trem2$^{+/+}$ CDMCs versus control samples (Figures 5F–5I and S5D). These results suggest that restoration of Trem2 function by wild-type CDMC transplantation results in re-expression of Syk signaling-dependent genes, as well as other Syk-mediated signaling receptors, including Clec7a and CD11c.

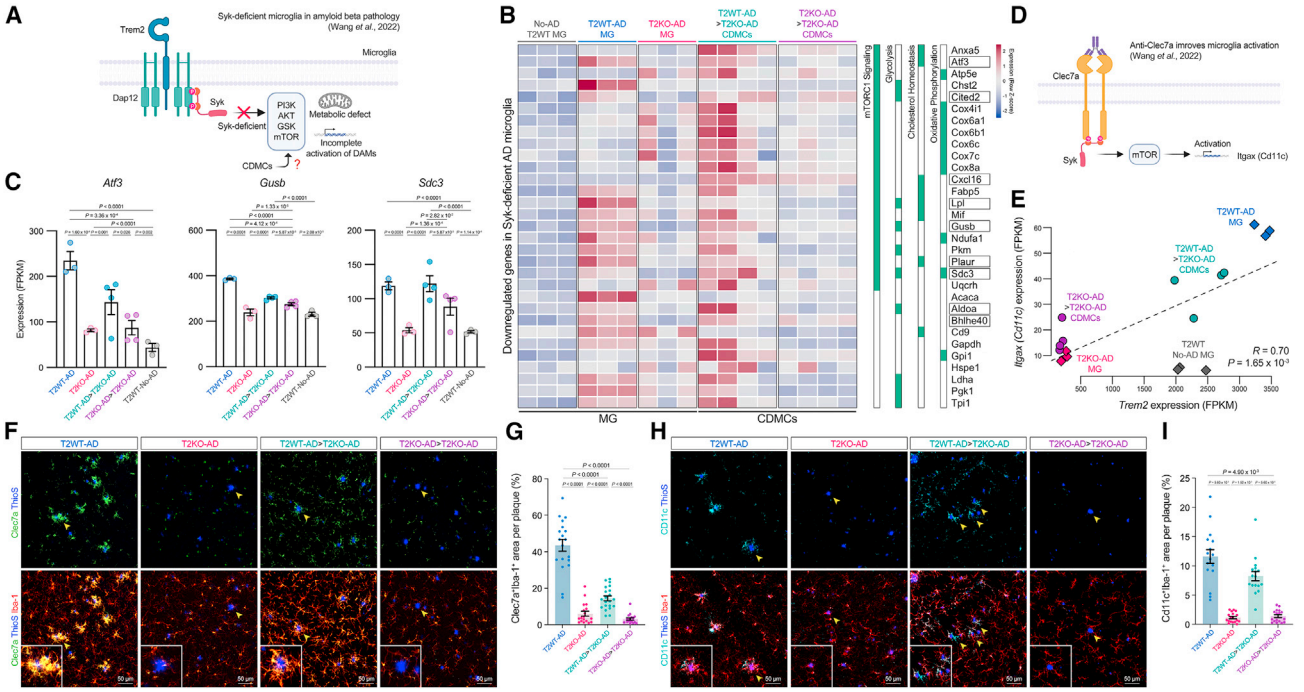


Figure 5. Increased expression of Syk-dependent genes and Clec7a following replacement of Trem2$^{-/-}$ 5xFAD microglia with Trem2$^{+/+}$ CDMCs

(A) Schematic figure summarizing the Syk-dependent pathway in microglia.[43,44,50,53]

(B) Heatmap showing the expression of 31 genes that downregulated in Syk-deficient AD microglia.[50] Significantly elevated Syk-dependent genes in Trem2$^{+/+}$ CDMCs were highlighted with box.

(C) Read counts (FPKM) from RNA-seq for *Atf3*, *Gusb*, and *Sdc3*.

(D) Schematic figure summarizing the microglia activation via anti-Clec7a treatment.[50]

(E) Correlation plot of *Trem2* expression with *Cd11c* expression in RNA-seq. *R*, correlation coefficient; *P*, p value for linear regression analysis.

(F) Representative confocal images of Clec7a$^+$ (green), Iba-1$^+$ (red), and ThioS-labeled Aβ plaques (blue). Arrowheads indicate objects shown in insets in higher magnification.

(G) Quantification of the Clec7a$^+$ Iba-1$^+$ area within 15 μm from the edge of each plaque. Data points are from representative 18–20 plaques from n = 4–6 mice per group.

(H) Restoration of plaque-enriched Cd11c expression after CDMC transplantation as shown by confocal immunofluorescence microscopy of Iba-1$^+$ (red), Cd11c$^+$ (cyan), and ThioS-labeled Aβ plaques (blue) in the cortex. Arrowheads indicate objects shown in insets in higher magnification.

(I) Quantification of the Cd11c$^+$ Iba-1$^+$ area within 15 μm from the edge of each plaque. Data points represent the average of n = 4–5 per group, three brain slices per animal.

Statistical significance between groups was calculated by Wald test in DESeq2 package (C) and two-tailed unpaired Student's t test (G and I). Data are presented as mean ± SEM. Exact p values were indicated. MG, microglia.

DISCUSSION

The role of TREM2 in the molecular pathogenesis of AD has been a central research focus in recent years but remains unclear to date. Human genetics provides compelling evidence that *TREM2* loss of function is causing neurodegeneration.[6–10] Furthermore, studies in both mouse and human models demonstrated that Trem2 is required for the DAM transcriptional response.[28,36] These results suggest that the DAM response, despite its disease association, is in fact neuroprotective, although a recent nuclear sequencing study showed a partial activation of DAM genes in the human postmortem brain of TREM2^{R47H} carriers and in mice carrying a human TREM2^{R47H} knockin allele.[57] Given these data, it is quite confusing that Trem2 loss of function in mice does not cause neurodegeneration[58] and does not have behavioral phenotypes with[59] or without[60] the 5xFAD background. This illustrates potential species differences of Trem2 biology or potential compensation mechanisms in mice that are absent in humans. Perhaps even more confusing is the observation that Trem2 mutations are neuroprotective in Tau mouse models.[24,61] When combined with various AD-associated APP mutations, it is, however, very clear that Trem2 is necessary for microglia to engage with Aβ plaques and affect their appearance and number.[23,26,30] Despite these many uncertainties, there is little doubt that restoring physiological Trem2 function in patients carrying Trem2 mutations would be therapeutic. Recent studies demonstrated that enhancing Trem2 activity is beneficial even in mouse AD models in a Trem2 wild-type context.[59,62]

We and others have recently developed a hematopoietic cell transplantation procedure to replace microglia with grafted myeloid cells in high efficiency.[14,15,63–65] Such high-efficiency microglia replacement would represent an attractive way to replace dysfunctional microglia with normal or even enhanced

Trem2 activity. Importantly, though, peripheral myeloid cells incorporated into the normal brain are slightly distinct from endogenous microglia.[14,15] Their moderately altered function could have a detrimental effect on neurodegeneration. Corroborating our findings, previous papers have shown that simple replacement of microglia with peripheral circulation-derived myeloid cells does not affect Aβ pathology in AD mouse models.[19] Thus, microglia replacement per se appears not to promote neurodegeneration and thus remains attractive to restore Trem2 function. Indeed, we could demonstrate a clear beneficial effect of replacing Trem2 mutant microglia with Trem2 wild-type myeloid cells in an Aβ mouse model. All microglial phenotypes and hallmarks of Aβ pathology caused by Trem2 deficiency were rectified. These findings show the proof of concept that a hematopoietic cell therapy is effective in restoring Trem2 function.

Currently, hematopoietic cell transplantation requires toxic preconditioning of the bone marrow niche precluding its application in chronic, non-life-threatening diseases, but promising efforts are underway to accomplish non-toxic preconditioning.[66,67] Given the strong scientific rationale of Trem2 to prevent neurodegeneration, high-efficiency microglia replacement may thus represent a viable option to treat AD in the future.

Limitations of the study

It is important to point out that the restoration of Trem2 function by replacing Trem2-deficient microglia at 8 weeks of age, which is about the time when histopathological abnormalities develop in these mice, led to much less-pronounced effects on Aβ load than when cells were transplanted at 3 weeks of age. This suggests that Trem2$^{+/+}$ CDMCs may primarily prevent the formation of new plaques. Another open aspect is whether replacement of Trem2-deficient microglia at an early age may contribute to other neurodevelopment-related phenotypes, as CDMCs are not identical to microglia. Finally, future studies are needed to better understand functional consequences of Clec7a or Syk depletion in CDMCs, as well as whether Trem2 and Clec7a/Syk pathways are independent in CDMCs. Although previous *in vitro*[44] and *in vivo*[49,50] studies have shown that Trem2 activation can activate the Syk signaling pathway, it still remains to be seen whether Trem2 relies solely on Syk to regulate its effects, especially in CDMCs. While our study showed CD11c induction in CDMCs, which is thought to be a microglial activation marker via Clec7a pathway,[50] further investigations are needed to better understand whether activation of the Trem2 and Clec7a pathway is mutually necessary for AD progression in amyloid pathology.

STAR★METHODS

Detailed methods are provided in the online version of this paper and include the following:

- KEY RESOURCES TABLE
- RESOURCE AVAILABILITY
  - Lead contact
  - Materials availability
  - Data and code availability
- EXPERIMENTAL MODELS AND STUDY PARTICIPANT DETAILS
  - Mice
- METHOD DETAILS
  - PLX5622 treatment
  - Brain sample preparation
  - Flow cytometry
  - Peripheral blood (PB) analysis
  - Immunofluorescence microscopy
  - Image analysis
  - RNA isolation, cDNA synthesis, quantitative RT-PCR (qPCR)
  - Droplet digital PCR (ddPCR)
  - RNA-sequencing analysis
- QUANTIFICATION AND STATISTICAL ANALYSIS

SUPPLEMENTAL INFORMATION

Supplemental information can be found online at https://doi.org/10.1016/j.stem.2023.07.006.

ACKNOWLEDGMENTS

We would like to thank the FACS core at the Institute for Stem Cell Biology and Regenerative Medicine of Stanford University, the Protein and Nucleic Acid (PAN) Biotechnology Facility of Stanford University, the Stanford Research Computing Center, and Wu Tsai Neuroscience Institute Neuroscience Microscopy Service of Stanford University for their microscopy assistance, expertise, and services. This work was supported by the Kleberg Foundation, the Emerson Collective, and a Howard Hughes Medical Institute Faculty Scholar Award; Y.Y. was supported by the New York Stem Cell Foundation Druckenmiller Fellowship (NYSCF-D-F74) and Postdoctoral Overseas Training Fellowship of National Research Foundation of Korea (2020R1A6A3A03039573); M.M. was supported by the German Research Foundation (Deutsche Forschungsgemeinschaft, DFG, MA 8492/1-1).

AUTHOR CONTRIBUTIONS

Y.Y. and M.W. were responsible for the conception, design, and interpretation of the experiments and wrote the manuscript. Y.Y., Y.S., and M.M. performed mice experiments; G.N. performed and analyzed droplet digital PCR experiment; Y.Y. performed and analyzed RNA-seq analysis; Y.Y. and M.W. wrote the manuscript; all authors reviewed, revised, and approved the final version of the paper.

DECLARATION OF INTERESTS

The authors declare no conflict of interest related to this study.

INCLUSION AND DIVERSITY

We support inclusive, diverse, and equitable conduct of research.

Received: January 15, 2023
Revised: May 10, 2023
Accepted: July 11, 2023
Published: August 3, 2023; corrected online: August 29, 2023

REFERENCES

1. Querfurth, H.W., and LaFerla, F.M. (2010). Alzheimer's disease. N. Engl. J. Med. *362*, 329–344. https://doi.org/10.1056/NEJMra0909142.
2. Tanzi, R.E., and Bertram, L. (2005). Twenty years of the Alzheimer's disease amyloid hypothesis: a genetic perspective. Cell *120*, 545–555. https://doi.org/10.1016/j.cell.2005.02.008.
3. Haass, C., and Selkoe, D. (2022). If amyloid drives Alzheimer disease, why have anti-amyloid therapies not yet slowed cognitive decline? PLoS Biol. *20*, e3001694. https://doi.org/10.1371/journal.pbio.3001694.

4. Morris, G.P., Clark, I.A., and Vissel, B. (2014). Inconsistencies and controversies surrounding the amyloid hypothesis of Alzheimer's disease. Acta Neuropathol. Commun. *2*, 135. https://doi.org/10.1186/s40478-014-0135-5.

5. Kunkle, B.W., Grenier-Boley, B., Sims, R., Bis, J.C., Damotte, V., Naj, A.C., Boland, A., Vronskaya, M., van der Lee, S.J., Amlie-Wolf, A., et al. (2019). Genetic meta-analysis of diagnosed Alzheimer's disease identifies new risk loci and implicates Abeta, tau, immunity and lipid processing. Nat. Genet. *51*, 414–430. https://doi.org/10.1038/s41588-019-0358-2.

6. Guerreiro, R., Wojtas, A., Bras, J., Carrasquillo, M., Rogaeva, E., Majounie, E., Cruchaga, C., Sassi, C., Kauwe, J.S.K., Younkin, S., et al. (2013). TREM2 variants in Alzheimer's disease. N. Engl. J. Med. *368*, 117–127. https://doi.org/10.1056/NEJMoa1211851.

7. Jonsson, T., Stefansson, H., Steinberg, S., Jonsdottir, I., Jonsson, P.V., Snaedal, J., Bjornsson, S., Huttenlocher, J., Levey, A.I., Lah, J.J., et al. (2013). Variant of TREM2 associated with the risk of Alzheimer's disease. N. Engl. J. Med. *368*, 107–116. https://doi.org/10.1056/NEJMoa1211103.

8. Paloneva, J., Autti, T., Raininko, R., Partanen, J., Salonen, O., Puranen, M., Hakola, P., and Haltia, M. (2001). CNS manifestations of Nasu-Hakola disease: a frontal dementia with bone cysts. Neurology *56*, 1552–1558. https://doi.org/10.1212/wnl.56.11.1552.

9. Chouery, E., Delague, V., Bergougnoux, A., Koussa, S., Serre, J.L., and Mégarbané, A. (2008). Mutations in TREM2 lead to pure early-onset dementia without bone cysts. Hum. Mutat. *29*, E194–E204. https://doi.org/10.1002/humu.20836.

10. Bianchin, M.M., Martin, K.C., de Souza, A.C., de Oliveira, M.A., and Rieder, C.R.d.M. (2010). Nasu-Hakola disease and primary microglial dysfunction. Nat. Rev. Neurol. *6*, 2. https://doi.org/10.1038/nrneurol.2010.17-c1.

11. Richard, B.C., Kurdakova, A., Baches, S., Bayer, T.A., Weggen, S., and Wirths, O. (2015). Gene Dosage Dependent Aggravation of the Neurological Phenotype in the 5XFAD Mouse Model of Alzheimer's Disease. J. Alzheimers Dis. *45*, 1223–1236. https://doi.org/10.3233/JAD-143120.

12. Oakley, H., Cole, S.L., Logan, S., Maus, E., Shao, P., Craft, J., Guillozet-Bongaarts, A., Ohno, M., Disterhoft, J., Van Eldik, L., et al. (2006). Intraneuronal beta-amyloid aggregates, neurodegeneration, and neuron loss in transgenic mice with five familial Alzheimer's disease mutations: potential factors in amyloid plaque formation. J. Neurosci. *26*, 10129–10140. https://doi.org/10.1523/JNEUROSCI.1202-06.2006.

13. Liu, S., Lockhart, J.R., Fontenard, S., Berlett, M., and Ryan, T.M. (2020). Mapping the Chromosomal Insertion Site of the GFP Transgene of UBC-GFP Mice to the MHC Locus. J. Immunol. *204*, 1982–1987. https://doi.org/10.4049/jimmunol.1901338.

14. Cronk, J.C., Filiano, A.J., Louveau, A., Marin, I., Marsh, R., Ji, E., Goldman, D.H., Smirnov, I., Geraci, N., Acton, S., et al. (2018). Peripherally derived macrophages can engraft the brain independent of irradiation and maintain an identity distinct from microglia. J. Exp. Med. *215*, 1627–1647. https://doi.org/10.1084/jem.20180247.

15. Shibuya, Y., Kumar, K.K., Mader, M.M.D., Yoo, Y., Ayala, L.A., Zhou, M., Mohr, M.A., Neumayer, G., Kumar, I., Yamamoto, R., et al. (2022). Treatment of a genetic brain disease by CNS-wide microglia replacement. Sci. Transl. Med. *14*, eabl9945. https://doi.org/10.1126/scitranslmed.abl9945.

16. Condello, C., Yuan, P., Schain, A., and Grutzendler, J. (2015). Microglia constitute a barrier that prevents neurotoxic protofibrillar Abeta42 hotspots around plaques. Nat. Commun. *6*, 6176. https://doi.org/10.1038/ncomms7176.

17. Yuan, P., Condello, C., Keene, C.D., Wang, Y., Bird, T.D., Paul, S.M., Luo, W., Colonna, M., Baddeley, D., and Grutzendler, J. (2016). TREM2 Haplodeficiency in Mice and Humans Impairs the Microglia Barrier Function Leading to Decreased Amyloid Compaction and Severe Axonal Dystrophy. Neuron *92*, 252–264. https://doi.org/10.1016/j.neuron.2016.09.016.

18. Parakalan, R., Jiang, B., Nimmi, B., Janani, M., Jayapal, M., Lu, J., Tay, S.S.W., Ling, E.A., and Dheen, S.T. (2012). Transcriptome analysis of amoeboid and ramified microglia isolated from the corpus callosum of rat brain. BMC Neurosci. *13*, 64. https://doi.org/10.1186/1471-2202-13-64.

19. Varvel, N.H., Grathwohl, S.A., Degenhardt, K., Resch, C., Bosch, A., Jucker, M., and Neher, J.J. (2015). Replacement of brain-resident myeloid cells does not alter cerebral amyloid-beta deposition in mouse models of Alzheimer's disease. J. Exp. Med. *212*, 1803–1809. https://doi.org/10.1084/jem.20150478.

20. Prokop, S., Miller, K.R., Drost, N., Handrick, S., Mathur, V., Luo, J., Wegner, A., Wyss-Coray, T., and Heppner, F.L. (2015). Impact of peripheral myeloid cells on amyloid-beta pathology in Alzheimer's disease-like mice. J. Exp. Med. *212*, 1811–1818. https://doi.org/10.1084/jem.20150479.

21. Ulrich, J.D., Finn, M.B., Wang, Y., Shen, A., Mahan, T.E., Jiang, H., Stewart, F.R., Piccio, L., Colonna, M., and Holtzman, D.M. (2014). Altered microglial response to Abeta plaques in APPPS1-21 mice heterozygous for TREM2. Mol. Neurodegener. *9*, 20. https://doi.org/10.1186/1750-1326-9-20.

22. Song, W., Hooli, B., Mullin, K., Jin, S.C., Cella, M., Ulland, T.K., Wang, Y., Tanzi, R.E., and Colonna, M. (2017). Alzheimer's disease-associated TREM2 variants exhibit either decreased or increased ligand-dependent activation. Alzheimers Dement. *13*, 381–387. https://doi.org/10.1016/j.jalz.2016.07.004.

23. Song, W.M., Joshita, S., Zhou, Y., Ulland, T.K., Gilfillan, S., and Colonna, M. (2018). Humanized TREM2 mice reveal microglia-intrinsic and -extrinsic effects of R47H polymorphism. J. Exp. Med. *215*, 745–760. https://doi.org/10.1084/jem.20171529.

24. Leyns, C.E.G., Ulrich, J.D., Finn, M.B., Stewart, F.R., Koscal, L.J., Remolina Serrano, J., Robinson, G.O., Anderson, E., Colonna, M., and Holtzman, D.M. (2017). TREM2 deficiency attenuates neuroinflammation and protects against neurodegeneration in a mouse model of tauopathy. Proc. Natl. Acad. Sci. USA *114*, 11524–11529. https://doi.org/10.1073/pnas.1710311114.

25. Jay, T.R., Miller, C.M., Cheng, P.J., Graham, L.C., Bemiller, S., Broihier, M.L., Xu, G., Margevicius, D., Karlo, J.C., Sousa, G.L., et al. (2015). TREM2 deficiency eliminates TREM2+ inflammatory macrophages and ameliorates pathology in Alzheimer's disease mouse models. J. Exp. Med. *212*, 287–295. https://doi.org/10.1084/jem.20142322.

26. Wang, Y., Cella, M., Mallinson, K., Ulrich, J.D., Young, K.L., Robinette, M.L., Gilfillan, S., Krishnan, G.M., Sudhakar, S., Zinselmeyer, B.H., et al. (2015). TREM2 lipid sensing sustains the microglial response in an Alzheimer's disease model. Cell *160*, 1061–1071. https://doi.org/10.1016/j.cell.2015.01.049.

27. Wang, Y., Ulland, T.K., Ulrich, J.D., Song, W., Tzaferis, J.A., Hole, J.T., Yuan, P., Mahan, T.E., Shi, Y., Gilfillan, S., et al. (2016). TREM2-mediated early microglial response limits diffusion and toxicity of amyloid plaques. J. Exp. Med. *213*, 667–675. https://doi.org/10.1084/jem.20151948.

28. Keren-Shaul, H., Spinrad, A., Weiner, A., Matcovitch-Natan, O., Dvir-Szternfeld, R., Ulland, T.K., David, E., Baruch, K., Lara-Astaiso, D., Toth, B., et al. (2017). A Unique Microglia Type Associated with Restricting Development of Alzheimer's Disease. Cell *169*, 1276–1290.e17. https://doi.org/10.1016/j.cell.2017.05.018.

29. Colonna, M., and Wang, Y. (2016). TREM2 variants: new keys to decipher Alzheimer disease pathogenesis. Nat. Rev. Neurosci. *17*, 201–207. https://doi.org/10.1038/nrn.2016.7.

30. Parhizkar, S., Arzberger, T., Brendel, M., Kleinberger, G., Deussing, M., Focke, C., Nuscher, B., Xiong, M., Ghasemigharagoz, A., Katzmarski, N., et al. (2019). Loss of TREM2 function increases amyloid seeding but reduces plaque-associated ApoE. Nat. Neurosci. *22*, 191–204. https://doi.org/10.1038/s41593-018-0296-9.

31. Walker, D.G., and Lue, L.F. (2015). Immune phenotypes of microglia in human neurodegenerative disease: challenges to detecting microglial

polarization in human brains. Alzheimer's Res. Ther. *7*, 56. https://doi.org/10.1186/s13195-015-0139-9.

32. Gratuze, M., Leyns, C.E., Sauerbeck, A.D., St-Pierre, M.K., Xiong, M., Kim, N., Serrano, J.R., Tremblay, M.È., Kummer, T.T., Colonna, M., et al. (2020). Impact of TREM2R47H variant on tau pathology-induced gliosis and neurodegeneration. J. Clin. Invest. *130*, 4954–4968. https://doi.org/10.1172/JCI138179.
33. Leyns, C.E.G., Gratuze, M., Narasimhan, S., Jain, N., Koscal, L.J., Jiang, H., Manis, M., Colonna, M., Lee, V.M.Y., Ulrich, J.D., and Holtzman, D.M. (2019). TREM2 function impedes tau seeding in neuritic plaques. Nat. Neurosci. *22*, 1217–1222. https://doi.org/10.1038/s41593-019-0433-0.
34. Fitz, N.F., Wolfe, C.M., Playso, B.E., Biedrzycki, R.J., Lu, Y., Nam, K.N., Lefterov, I., and Koldamova, R. (2020). Trem2 deficiency differentially affects phenotype and transcriptome of human APOE3 and APOE4 mice. Mol. Neurodegener. *15*, 41. https://doi.org/10.1186/s13024-020-00394-4.
35. Gowrishankar, S., Yuan, P., Wu, Y., Schrag, M., Paradise, S., Grutzendler, J., De Camilli, P., and Ferguson, S.M. (2015). Massive accumulation of luminal protease-deficient axonal lysosomes at Alzheimer's disease amyloid plaques. Proc. Natl. Acad. Sci. USA *112*, E3699–E3708. https://doi.org/10.1073/pnas.1510329112.
36. McQuade, A., Kang, Y.J., Hasselmann, J., Jairaman, A., Sotelo, A., Coburn, M., Shabestari, S.K., Chadarevian, J.P., Fote, G., Tu, C.H., et al. (2020). Gene expression and functional deficits underlie TREM2-knockout microglia responses in human models of Alzheimer's disease. Nat. Commun. *11*, 5370. https://doi.org/10.1038/s41467-020-19227-5.
37. Gouna, G., Klose, C., Bosch-Queralt, M., Liu, L., Gokce, O., Schifferer, M., Cantuti-Castelvetri, L., and Simons, M. (2021). TREM2-dependent lipid droplet biogenesis in phagocytes is required for remyelination. J. Exp. Med. *218*, e20210227. https://doi.org/10.1084/jem.20210227.
38. Grubman, A., Choo, X.Y., Chew, G., Ouyang, J.F., Sun, G., Croft, N.P., Rossello, F.J., Simmons, R., Buckberry, S., Landin, D.V., et al. (2021). Transcriptional signature in microglia associated with Abeta plaque phagocytosis. Nat. Commun. *12*, 3015. https://doi.org/10.1038/s41467-021-23111-1.
39. Butovsky, O., Jedrychowski, M.P., Moore, C.S., Cialic, R., Lanser, A.J., Gabriely, G., Koeglsperger, T., Dake, B., Wu, P.M., Doykan, C.E., et al. (2014). Identification of a unique TGF-beta-dependent molecular and functional signature in microglia. Nat. Neurosci. *17*, 131–143. https://doi.org/10.1038/nn.3599.
40. Chiu, I.M., Morimoto, E.T.A., Goodarzi, H., Liao, J.T., O'Keeffe, S., Phatnani, H.P., Muratet, M., Carroll, M.C., Levy, S., Tavazoie, S., et al. (2013). A neurodegeneration-specific gene-expression signature of acutely isolated microglia from an amyotrophic lateral sclerosis mouse model. Cell Rep. *4*, 385–401. https://doi.org/10.1016/j.celrep.2013.06.018.
41. Zhou, Y., Song, W.M., Andhey, P.S., Swain, A., Levy, T., Miller, K.R., Poliani, P.L., Cominelli, M., Grover, S., Gilfillan, S., et al. (2020). Human and mouse single-nucleus transcriptomics reveal TREM2-dependent and TREM2-independent cellular responses in Alzheimer's disease. Nat. Med. *26*, 131–142. https://doi.org/10.1038/s41591-019-0695-9.
42. Mathys, H., Davila-Velderrain, J., Peng, Z., Gao, F., Mohammadi, S., Young, J.Z., Menon, M., He, L., Abdurrob, F., Jiang, X., et al. (2019). Single-cell transcriptomic analysis of Alzheimer's disease. Nature *570*, 332–337. https://doi.org/10.1038/s41586-019-1195-2.
43. Turner, M., Schweighoffer, E., Colucci, F., Di Santo, J.P., and Tybulewicz, V.L. (2000). Tyrosine kinase SYK: essential functions for immunoreceptor signalling. Immunol. Today *21*, 148–154. https://doi.org/10.1016/s0167-5699(99)01574-1.
44. Yao, H., Coppola, K., Schweig, J.E., Crawford, F., Mullan, M., and Paris, D. (2019). Distinct Signaling Pathways Regulate TREM2 Phagocytic and NFkappaB Antagonistic Activities. Front. Cell. Neurosci. *13*, 457. https://doi.org/10.3389/fncel.2019.00457.
45. Mócsai, A., Abram, C.L., Jakus, Z., Hu, Y., Lanier, L.L., and Lowell, C.A. (2006). Integrin signaling in neutrophils and macrophages uses adaptors containing immunoreceptor tyrosine-based activation motifs. Nat. Immunol. *7*, 1326–1333. https://doi.org/10.1038/ni1407.
46. Rogers, N.C., Slack, E.C., Edwards, A.D., Nolte, M.A., Schulz, O., Schweighoffer, E., Williams, D.L., Gordon, S., Tybulewicz, V.L., Brown, G.D., and Reis e Sousa, C. (2005). Syk-dependent cytokine induction by Dectin-1 reveals a novel pattern recognition pathway for C type lectins. Immunity *22*, 507–517. https://doi.org/10.1016/j.immuni.2005.03.004.
47. Wright, G.J., Cherwinski, H., Foster-Cuevas, M., Brooke, G., Puklavec, M.J., Bigler, M., Song, Y., Jenmalm, M., Gorman, D., McClanahan, T., et al. (2003). Characterization of the CD200 receptor family in mice and humans and their interactions with CD200. J. Immunol. *171*, 3034–3046. https://doi.org/10.4049/jimmunol.171.6.3034.
48. Yamanishi, Y., Kitaura, J., Izawa, K., Matsuoka, T., Oki, T., Lu, Y., Shibata, F., Yamazaki, S., Kumagai, H., Nakajima, H., et al. (2008). Analysis of mouse LMIR5/CLM-7 as an activating receptor: differential regulation of LMIR5/CLM-7 in mouse versus human cells. Blood *111*, 688–698. https://doi.org/10.1182/blood-2007-04-085787.
49. Ennerfelt, H., Frost, E.L., Shapiro, D.A., Holliday, C., Zengeler, K.E., Voithofer, G., Bolte, A.C., Lammert, C.R., Kulas, J.A., Ulland, T.K., and Lukens, J.R. (2022). SYK coordinates neuroprotective microglial responses in neurodegenerative disease. Cell *185*, 4135–4152.e22. https://doi.org/10.1016/j.cell.2022.09.030.
50. Wang, S., Sudan, R., Peng, V., Zhou, Y., Du, S., Yuede, C.M., Lei, T., Hou, J., Cai, Z., Cella, M., et al. (2022). TREM2 drives microglia response to amyloid-beta via SYK-dependent and -independent pathways. Cell *185*, 4153–4169.e19. https://doi.org/10.1016/j.cell.2022.09.033.
51. Loving, B.A., Tang, M., Neal, M.C., Gorkhali, S., Murphy, R., Eckel, R.H., and Bruce, K.D. (2021). Lipoprotein Lipase Regulates Microglial Lipid Droplet Accumulation. Cells *10*, 198. https://doi.org/10.3390/cells10020198.
52. Ma, Y., Bao, J., Zhao, X., Shen, H., Lv, J., Ma, S., Zhang, X., Li, Z., Wang, S., Wang, Q., and Ji, J. (2013). Activated cyclin-dependent kinase 5 promotes microglial phagocytosis of fibrillar beta-amyloid by up-regulating lipoprotein lipase expression. Mol. Cell. Proteomics *12*, 2833–2844. https://doi.org/10.1074/mcp.M112.026864.
53. Chu, D.H., Morita, C.T., and Weiss, A. (1998). The Syk family of protein tyrosine kinases in T-cell activation and development. Immunol. Rev. *165*, 167–180. https://doi.org/10.1111/j.1600-065x.1998.tb01238.x.
54. Herre, J., Marshall, A.S.J., Caron, E., Edwards, A.D., Williams, D.L., Schweighoffer, E., Tybulewicz, V., Reis e Sousa, C., Gordon, S., and Brown, G.D. (2004). Dectin-1 uses novel mechanisms for yeast phagocytosis in macrophages. Blood *104*, 4038–4045. https://doi.org/10.1182/blood-2004-03-1140.
55. Krasemann, S., Madore, C., Cialic, R., Baufeld, C., Calcagno, N., El Fatimy, R., Beckers, L., O'Loughlin, E., Xu, Y., Fanek, Z., et al. (2017). The TREM2-APOE Pathway Drives the Transcriptional Phenotype of Dysfunctional Microglia in Neurodegenerative Diseases. Immunity *47*, 566–581.e9. https://doi.org/10.1016/j.immuni.2017.08.008.
56. Underhill, D.M., Rossnagle, E., Lowell, C.A., and Simmons, R.M. (2005). Dectin-1 activates Syk tyrosine kinase in a dynamic subset of macrophages for reactive oxygen production. Blood *106*, 2543–2550. https://doi.org/10.1182/blood-2005-03-1239.
57. Sayed, F.A., Kodama, L., Fan, L., Carling, G.K., Udeochu, J.C., Le, D., Li, Q., Zhou, L., Wong, M.Y., Horowitz, R., et al. (2021). AD-linked R47H-TREM2 mutation induces disease-enhancing microglial states via AKT hyperactivation. Sci. Transl. Med. *13*, eabe3947. https://doi.org/10.1126/scitranslmed.abe3947.
58. Filipello, F., Morini, R., Corradini, I., Zerbi, V., Canzi, A., Michalski, B., Erreni, M., Markicevic, M., Starvaggi-Cucuzza, C., Otero, K., et al. (2018). The Microglial Innate Immune Receptor TREM2 Is Required for Synapse Elimination and Normal Brain Connectivity. Immunity *48*, 979–991.e8. https://doi.org/10.1016/j.immuni.2018.04.016.
59. Wang, S., Mustafa, M., Yuede, C.M., Salazar, S.V., Kong, P., Long, H., Ward, M., Siddiqui, O., Paul, R., Gilfillan, S., et al. (2020). Anti-human TREM2 induces microglia proliferation and reduces pathology in an

Alzheimer's disease model. J. Exp. Med. *217*, e20200785. https://doi.org/10.1084/jem.20200785.

60. Kang, S.S., Kurti, A., Baker, K.E., Liu, C.C., Colonna, M., Ulrich, J.D., Holtzman, D.M., Bu, G., and Fryer, J.D. (2018). Behavioral and transcriptomic analysis of Trem2-null mice: not all knockout mice are created equal. Hum. Mol. Genet. *27*, 211–223. https://doi.org/10.1093/hmg/ddx366.
61. Sayed, F.A., Telpoukhovskaia, M., Kodama, L., Li, Y., Zhou, Y., Le, D., Hauduc, A., Ludwig, C., Gao, F., Clelland, C., et al. (2018). Differential effects of partial and complete loss of TREM2 on microglial injury response and tauopathy. Proc. Natl. Acad. Sci. USA *115*, 10172–10177. https://doi.org/10.1073/pnas.1811411115.
62. Peng, Q., Malhotra, S., Torchia, J.A., Kerr, W.G., Coggeshall, K.M., and Humphrey, M.B. (2010). TREM2- and DAP12-dependent activation of PI3K requires DAP10 and is inhibited by SHIP1. Sci. Signal. *3*, ra38. https://doi.org/10.1126/scisignal.2000500.
63. Hohsfield, L.A., Najafi, A.R., Ghorbanian, Y., Soni, N., Hingco, E.E., Kim, S.J., Jue, A.D., Swarup, V., Inlay, M.A., and Green, K.N. (2020). Effects of long-term and brain-wide colonization of peripheral bone marrow-derived myeloid cells in the CNS. J. Neuroinflammation *17*, 279. https://doi.org/10.1186/s12974-020-01931-0.
64. Xu, Z., Rao, Y., Huang, Y., Zhou, T., Feng, R., Xiong, S., Yuan, T.F., Qin, S., Lu, Y., Zhou, X., et al. (2020). Efficient Strategies for Microglia Replacement in the Central Nervous System. Cell Rep. *32*, 108041. https://doi.org/10.1016/j.celrep.2020.108041.
65. Xu, Z., Zhou, X., Peng, B., and Rao, Y. (2021). Microglia replacement by bone marrow transplantation (Mr BMT) in the central nervous system of adult mice. STAR Protoc. *2*, 100666. https://doi.org/10.1016/j.xpro.2021.100666.
66. Kwon, H.S., Logan, A.C., Chhabra, A., Pang, W.W., Czechowicz, A., Tate, K., Le, A., Poyser, J., Hollis, R., Kelly, B.V., et al. (2019). Anti-human CD117 antibody-mediated bone marrow niche clearance in nonhuman primates and humanized NSG mice. Blood *133*, 2104–2108. https://doi.org/10.1182/blood-2018-06-853879.
67. Czechowicz, A., Palchaudhuri, R., Scheck, A., Hu, Y., Hoggatt, J., Saez, B., Pang, W.W., Mansour, M.K., Tate, T.A., Chan, Y.Y., et al. (2019). Selective hematopoietic stem cell ablation using CD117-antibody-drug-conjugates enables safe and effective transplantation with immunity preservation. Nat. Commun. *10*, 617. https://doi.org/10.1038/s41467-018-08201-x.
68. Huang, Y., Happonen, K.E., Burrola, P.G., O'Connor, C., Hah, N., Huang, L., Nimmerjahn, A., and Lemke, G. (2021). Microglia use TAM receptors to detect and engulf amyloid beta plaques. Nat. Immunol. *22*, 586–594. https://doi.org/10.1038/s41590-021-00913-5.
69. Pfaffl, M.W., Horgan, G.W., and Dempfle, L. (2002). Relative expression software tool (REST) for group-wise comparison and statistical analysis of relative expression results in real-time PCR. Nucleic Acids Res. *30*, e36. https://doi.org/10.1093/nar/30.9.e36.
70. Wang, X., Spandidos, A., Wang, H., and Seed, B. (2012). PrimerBank: a PCR primer database for quantitative gene expression analysis, 2012 update. Nucleic Acids Res. *40*, D1144–D1149. https://doi.org/10.1093/nar/gkr1013.
71. Anders, S., Pyl, P.T., and Huber, W. (2015). HTSeq–a Python framework to work with high-throughput sequencing data. Bioinformatics *31*, 166–169. https://doi.org/10.1093/bioinformatics/btu638.
72. Li, B., and Dewey, C.N. (2011). RSEM: accurate transcript quantification from RNA-Seq data with or without a reference genome. BMC Bioinf. *12*, 323. https://doi.org/10.1186/1471-2105-12-323.
73. Love, M.I., Huber, W., and Anders, S. (2014). Moderated estimation of fold change and dispersion for RNA-seq data with DESeq2. Genome Biol. *15*, 550. https://doi.org/10.1186/s13059-014-0550-8.
74. Raudvere, U., Kolberg, L., Kuzmin, I., Arak, T., Adler, P., Peterson, H., and Vilo, J. (2019). g:Profiler: a web server for functional enrichment analysis and conversions of gene lists (2019 update). Nucleic Acids Res. *47*, W191–W198. https://doi.org/10.1093/nar/gkz369.
75. Srinivasan, K., Friedman, B.A., Etxeberria, A., Huntley, M.A., van der Brug, M.P., Foreman, O., Paw, J.S., Modrusan, Z., Beach, T.G., Serrano, G.E., and Hansen, D.V. (2020). Alzheimer's Patient Microglia Exhibit Enhanced Aging and Unique Transcriptional Activation. Cell Rep. *31*, 107843. https://doi.org/10.1016/j.celrep.2020.107843.

STAR★METHODS

KEY RESOURCES TABLE

REAGENT or RESOURCE	SOURCE	IDENTIFIER
Antibodies		
Rat monoclonal anti-Trem2	R&D Systems	Cat# MAB17291; RRID: AB_2208679
Rabbit polyclonal anti-Trem2	Invitrogen	Cat# PA5-87933; RRID: AB_2804516
Rabbit polyclonal anti-Iba1	Wako Chemicals	Cat# 019–19741; RRID: AB_839504
Mouse monoclonal anti- β-Amyloid, 1–16 (6E10)	BioLegend	Cat# 803004; RRID: AB_2715854
Chicken polyclonal anti-GFP	Abcam	Cat# ab13970; RRID: AB_300798
Rat monoclonal anti-Cd68	Invitrogen	Cat# 14-0681-82; RRID: AB_2572857
Rat monoclonal anti-mDectin-1 (Clec7a)	InvivoGen	Cat# mabg-mdect; RRID: AB_2753143
Rabbit monoclonal anti-Lamp1	Abcam	Cat# ab208943; RRID: AB_2923327
Armenian Hamster monoclonal anti-CD11c	Novus	Cat# AP-MAB0806; RRID: AB_1290725
Rat monoclonal anti-CD11b-PE	BioLegend	Cat# 101208; RRID: AB_356991
Rat monoclonal anti-CD45-APC	BioLegend	Cat# 103112; RRID: AB_2176274
Rat monoclonal anti-Trem2-APC	R&D Systems	Cat# MAB17291; RRID: AB_2208679
Goat anti-chicken IgY (H+L) Antibody, Alexa Fluor 488 Conjugated	Thermo Fisher Scientific	Cat# A-11039; RRID: AB_2534096
Donkey anti-rabbit IgG (H+L) Antibody, Alexa Fluor 488 Conjugated	Thermo Fisher Scientific	Cat# A-21206; RRID: AB_2535792
Donkey anti-rabbit IgG (H+L) Antibody, Alexa Fluor 555 Conjugated	Thermo Fisher Scientific	Cat# A-31572; RRID: AB_162543
Donkey anti-goat IgG (H+L) Antibody, Alexa Fluor 555 Conjugated	Thermo Fisher Scientific	Cat# A-21432; RRID: AB_2535853
Donkey anti-mouse IgG (H+L) Antibody, Alexa Fluor 555 Conjugated	Thermo Fisher Scientific	Cat# A-31570; RRID: AB_2536180
Donkey anti-rat IgG (H+L) Antibody, Alexa Fluor 594 Conjugated	Thermo Fisher Scientific	Cat# A-21209; RRID: AB_2535795
Donkey anti-rabbit IgG (H+L) Antibody, Alexa Fluor 647 Conjugated	Thermo Fisher Scientific	Cat# A-31573; RRID: AB_2536183
Donkey anti-mouse IgG (H+L) Antibody, Alexa Fluor 647 Conjugated	Thermo Fisher Scientific	Cat# A-31571; RRID: AB_162542
Chemicals, peptides, and recombinant proteins		
REDExtract-N-Amp™ PCR ReadyMix	Sigma-Aldrich	Cat# R4775
Neural Tissue Dissociation Kit (P)	Miltenyi Biotec	Cat# 130-092-628
PLX5622	Plexxikon	N/A
Red blood cell lysis buffer	e-bioscience	Cat# 00-4300-54
Flow Cytometry Staining Buffer	e-bioscience	Cat# 00-4222-26
Busulfan	Sigma-Aldrich	Cat# B2635
Thioflavin S	Sigma-Aldrich	Cat# T1892
Triton X-100	Sigma-Aldrich	Cat# T8787
Sucrose	Sigma-Aldrich	Cat# S0389
DAPI	Sigma-Aldrich	Cat# 32670
DAPI Fluoromount-G	Southern Biotechnology	Cat# 0100-20
ProLong Gold Antifade Mountant	Thermo Fisher Scientific	Cat# P36930
HBSS, no calcium, no magnesium, no phenol red	Thermo Fisher Scientific	Cat# 14175095
HBSS, calcium, magnesium, no phenol red	Thermo Fisher Scientific	Cat# 14025092

(*Continued on next page*)

Continued

REAGENT or RESOURCE	SOURCE	IDENTIFIER
Percoll	Cytiva	Cat# 17089102
RNeasy MinElute Cleanup Kit	Qiagen	Cat# 74204
SMART-Seq® v4 Ultra® Low Input RNA Kit	Takara Bio	Cat# 634890
SuperScript III Reverse Transcriptase	Thermo Fisher Scientific	Cat# 18080044
SYBR Green PCR Master Mix	Thermo Fisher Scientific	Cat# 4309155
UltraPure 0.5M EDTA, pH 8.0	Thermo Fisher Scientific	Cat# 15575020
Quick-DNA Miniprep Kit	Zymo Research	Cat# D3024
TRIzol	Life Technologies	Cat# 15596018
Chloroform	Sigma-Aldrich	Cat# 288306
Isopropanol	Sigma-Aldrich	Cat# I9516
Paraformaldehyde Solution, 4% in PBS	Thermo Fisher Scientific	Cat# AAJ19943K2
2,2,2-Tribromoethanol (Avertin)	Sigma-Aldrich	Cat# T48402
Tissue-Tek™ CRYO-OCT Compound	Thermo Fisher Scientific	Cat# 14-373-65
Sodium Azide	Sigma-Aldrich	Cat# S2002
HyClone Cosmic Calf Serum	Cytiva	Cat# SH30087
Donkey Serum	Sigma-Aldrich	Cat# S30
Tween 20	Sigma-Aldrich	Cat# 11332465001
ddPCR Supermix for Probes (No dUTP)	BioRad	Cat# 1863025
DG8™ Cartridges for QX200™/QX100™ Droplet Generator	BioRad	Cat# 1864008
DG8™ Gaskets for QX200™/QX100™ Droplet Generator	BioRad	Cat# 1863009
Droplet Generation Oil for Probes	BioRad	Cat# 1863005
Eppendorf™ 96-Well Twin.tec™ PCR Plates	Fisher Scientific	Cat# E951020346
PCR Plate Heat Seal, foil, pierceable	BioRad	Cat# 1814040
Deposited data		
Gene expression data	This paper	GEO: GSE235607 https://www.ncbi.nlm.nih.gov/geo/query/acc.cgi?acc=GSE235607
Original code	This paper	Zenodo: https://doi.org/10.5281/zenodo.8117804
Experimental models: Organisms/strains		
C57BL/6J	The Jackson Laboratory	Strain# 000664; RRID: IMSR_JAX:000664
C57BL/6-Tg(UBC-GFP)30Scha/J	The Jackson Laboratory	Strain# 004353; RRID: IMSR_JAX:004353
B6SJL-Tg(APPSwFlLon, PSEN1*M146L*L286V)6799Vas/Mmjax	The Jackson Laboratory	MMRRC Strain# 034840-JAX
C57BL/6J-Trem2^{em2Adiuj}/J	The Jackson Laboratory	Strain# 027197; RRID: IMSR_JAX:027197
Software and algorithms		
Fiji	Fiji	RRID: SCR_002285
Imaris	Bitplane	RRID: SCR_007370
R Project for Statistical Computing	R software	RRID: SCR_001905
FlowJo Software	FlowJo	RRID:SCR_008520
Adobe Illustrator	Adobe	https://www.adobe.com/products/illustrator
Graphpad Prism 9	Graphpad Software	RRID: SCR_002798

RESOURCE AVAILABILITY

Lead contact

Further information and requests for resources and reagents should be directed to and will be fulfilled by the lead contact, Dr. Marius Wernig (wernig@stanford.edu).

Materials availability

All data are available in the main text or the Supplementary Materials. PLX5622 was provided by Plexxikon Inc. under a material transfer agreement between Stanford University and Plexxikon Inc.

Data and code availability

- Bulk RNA-seq data have been deposited at GEO and are publicly available as of the date of publication (accession number: GEO: GSE235607) and can be found in the key resources table.
- Original code for bulk RNA-seq analysis has been deposited at Zenodo and is publicly available as of the date of publication (Zenodo: https://doi.org/10.5281/zenodo.8117804) and is listed in the key resources table. Any additional information required to reanalyze the data reported in this paper will be shared by the lead contact upon request.

EXPERIMENTAL MODELS AND STUDY PARTICIPANT DETAILS

Mice

All animal studies and procedures were approved by the administrative panel on laboratory animal care at Stanford University. Age, sex-matched and immunocompetent mice were used, and all mice were group housed (up to five mice) under standard condition 12 h light/dark cycle with water and standard chow *ad libitum*. For PLX5622 treatment, mice were provided PLX5622-incorporated diet for the indicated time period in the text. All recipient mice aged 3weeks received microglia replacement (mrBMT), except for recipient mice subjected to 8weeks mrBMT experiments (Figures S4D and S4E). All age- and sex-matched donor cells, female-to-female, were used, except for samples subjected to droplet digital PCR (ddPCR) experiments. For ddPCR samples, we used male donor cells and recipient were all 3-week-old female mice. The number of animals used in each experiment is described in each figure legend. 5xFAD mice (Stock #034840-JAX) and *Trem2*$^{-/-}$ mice (Stock #027197-JAX) were obtained from The Jackson Laboratory and were crossed to generate *Trem2*$^{-/-}$; 5xFAD (denoted as T2KO-AD) experimental mice. Both, 5xFAD mice and T2KO-AD mice were also crossed with Ubc-GFP mice (Stock # 004353-JAX) to generate 5FAD; GFP (denoted as 5xFAD^{GFP}) and *Trem2*$^{-/-}$;5xFAD; GFP (denoted as T2KO-AD^{GFP}). After weaning at age of 3 weeks, T2WT and T2KO recipient mice received five intraperitoneal (IP) injections of busulfan (Sigma; Cat# B2635) at 25 mg/kg body weight per day for five days. On day 0, whole bone marrow cells (WBMCs) were isolated from tibias and femurs of T2WT-AD^{GFP}, T2WT-AD and T2KO-AD mice. Isolated WBMCs were resuspended in 1x red blood cell lysis buffer (e-bioscience; Cat# 00-4300-54) and incubated for 20 min at room temperature. WBMCs were passed through a 70 μm cell strainer, washed by applying 10 mL of ice-cold PBS and then resuspended in fresh PBS. WBMCs (5.0 x 10^6 in total) in 0.2 mL ice-cold PBS were injected into the retro-orbital sinus of pre-conditioned recipients as intravenous (IV) injection. On day 42 (at age of 6 weeks), the recipient mice were fed PLX5622 diet or control diet for 10 days and then returned to normal chow. Genotyping was performed by standard PCR using tail tip samples using REDExtract-N-Amp PCR ReadyMix (Sigma-Aldrich; Cat# R4775) with specific primers (Table S1).

METHOD DETAILS

PLX5622 treatment

PLX5622 was provided by Plexxikon Inc. under a Material Transfer Agreement and incorporated to AIN-76A standard chow by Research Diets Inc. at 1200 PPM. Mice were treated with PLX5622 or control diet *ad libitum* for the duration indicated in the figure legends.

Brain sample preparation

Mice were anesthetized using Avertin (20 mg/mL; IP; Sigma-Aldrich; Cat# T48402) and perfused via the left ventricle with ice-cold PBS without Ca^{2+} and Mg^{2+} for 6 min. Brains were removed and cut into two pieces along the midline. One hemisphere was immediately drop-fixed in 4% paraformaldehyde (Thermo Fisher Scientific; Cat# AAJ19943K2) for at least 48 h. Drop-fixed brain samples were transferred to 30% sucrose (Sigma-Aldrich; Cat# S0389) for 48 h and then mounted and frozen in Tissue-Plus OCT compound (Thermo Fisher Scientific; Cat# 14-373-65) and were then sectioned at 40 μm in thickness using a cryostat (Leica) and stored in PBS with 0.01% sodium azide (Sigma-Aldrich; Cat# S2002) at 4°C for immunofluorescence microscopy analysis. The other hemisphere was minced with a surgical knife, and then transferred to ice-cold HBSS without Ca^{2+} and Mg^{2+} (Thermo Fisher Scientific; Cat# 14175095). Minced hemi-brains were centrifuged at 300 x g for 5 min at room temperature and then enzymatically digested at 37°C for 35 min by using Neural Tissue Dissociation Kit P (Miltenyi Biotec; Cat# 130-092-628) according to the manufacturer's protocol. The cell suspension was passed through a 70 μm cell strainer and washed by applying 10 mL of HBSS with Ca^{2+} and Mg^{2+} (Thermo Fisher Scientific; Cat# 14025092) to the strainer. The cell suspension was centrifuged at 300 x g for 10 min at room temperature, re-suspended in 30% Percoll (Cytiva; Cat# 17089102), and then centrifuged at 700 x g with low decreasing speed for 10 min at 4°C. The supernatant containing the myelin was removed and the pellet was washed with 10 mL of HBSS with Ca^{2+} and Mg^{2+}. The resulting pellet was resuspended in flow cytometry staining buffer (e-bioscience; Cat# 00-4222-26) and subjected to antibody staining for flow cytometry analysis.

Flow cytometry

For flow cytometry analysis, cells were washed by flow cytometry staining buffer (e-bioscience; Cat# 00-4222-26) and centrifuged at 300 x g for 5 min and resuspended in 100 μL of staining buffer with fluorescently labeled antibodies specific for anti-CD45 (BioLegend; Cat# 103112; Clone 30-F11) and anti-CD11b (BioLegend; Cat# 101208; Clone M1/70) antibodies. Cells were incubated in the dark for 15–30 min at 4°C, washed with FACS staining buffer, and resuspended 1:5000 with DAPI (Sigma-Aldrich; Cat# 32670) in 500 μL of flow cytometry staining buffer. Microglia and CDMCs were identified as the CD11b and CD45 after gating for single and live cells using a BD FACSAria II. Post-acquisition analysis was performed using FlowJo software (FlowJo; RRID:SCR_008520).

Peripheral blood (PB) analysis

Approximately 50 μL of PB per mouse was collected from the retro-orbital venous sinus into 2.0 mL tubes containing 20 μL of 0.5M EDTA (Thermo Fisher Scientific; Cat# 15575020). Erythrocytes were removed with 1x red blood cell lysis buffer (e-bioscience; Cat# 00-4300-54) by incubating for 20 min at room temperature, and then cells were washed once with FACS staining buffer and resuspended 1:5000 with DAPI (Sigma-Aldrich; Cat# 32670) in 500 μL of FACS staining buffer. The PB chimerism was measured as the GFP^+ fraction of all live, $DAPI^-$ single cells using a BD FACSAria II.

Immunofluorescence microscopy

Sections were washed four times with PBS and processed for antibody staining. Brain sections were permeabilized and blocked with blocking buffer (2% donkey serum, 1% BSA, 0.1% Triton X-(Sigma-Aldrich; Cat# T8787), 0.05% Tween 20 (Sigma-Aldrich; Cat# 11332465001)) in PBS for 1 h at room temperature before applying the primary antibody master mix diluted in blocking solution overnight at 4°C. Samples were stained with anti-Aβ (6E10; BioLegend; Cat# 803004) to label amyloid plaques. To study microglial/CDMCs morphology and numbers, sections were stained with Iba-1 (Wako Chemicals; Cat# 019–19741) and GFP (Abcam, Cat# ab13970). To further characterize microglia or CDMCs, sections were labeled with Trem2 (R&D Systems; Cat# MAB17291), anti-CD68 (Invitrogen; Cat# 14-0681-82), anti-mDectin-1 (InvivoGen; Cat# mabg-mdect) and anti-Cd11c (Novus; Cat# AP-MAB0806). To access neuronal health, samples were stained with anti-Lamp1 (Abcam; Cat# ab208943). Sections were washed three times for 10 min at room temperature in PBS, then incubated in matched donkey Alexa Fluor 488, 594, 647 at room temperature for 2 h in dark. Samples were washed with again three times for 10 min at room temperature and incubated with DAPI (1:1000) for 10 min at room temperature. For staining for plaques with Thioflavin S (ThioS) (Sigma-Aldrich; 0.5%), free-floating sections were washed with PBS followed by dehydration in a graded series of ethanol (100%, 95%, 70%, 50%; 3 min each). The sections were then incubated in 0.5% ThioS in 50% ethanol for 10 mins, then sections were washed with 50% ethanol three times for 5 min followed by PBS washing for 10 min. Sections were dried, sealed with Fluoromount-G (Southern Biotech; Cat# 0100-20) and stored at 4°C. Images were obtained using a Zeiss LSM710/980plus confocal microscope or a Zeiss AxioImager motorized widefield fluorescence microscope. In confocal microscope, 11 z stack images (1024 × 1024 × 20 μm, 1 μm thickness) were acquired in random region of the cortices and hippocampi respectively. In widefield fluorescence microscope, images (2048 × 2048 μm) were obtained with 2.5× objective without z stack. Quantification of images were performed using Fiji software or Imaris software (Bitplane; 9.5.1).

Image analysis

For fixed-brain 40 μm sections, maximum-intensity projection images were analyzed in Fiji or Imaris software (Bitplane). Plaque-associated and non-plaque-associated Iba-1^+GFP^- microglia or Iba-1^+GFP^+ CDMCs areas were classified by investigator blind with respect to genotypes. Plaque-associated microglia or plaque-associated CDMCs were defined as those whose cell body centroids were 15 μm away from the edge of the nearest $ThioS^+/6E10^+$ edge of plaques.[16] On average 3–6 microglia or 2–4 CDMCs per plaque showed clear distinct process visibility. Primary process length and numbers of PAM or PAC were accessed using the 'free-hand' line tool in Fiji.[68] Mean fluorescence intensity of Trem2 was calculated as the quotient of integrated density divided by the region of interest. For amyloid plaques coverages, the $6E10^+$ area was calculated above a set fluorescent threshold using the Fiji 'analyze particle' tool. For quantification of single plaque size and circularity using $ThioS^+$, the area above a set fluorescent threshold for $ThioS^+$ area was calculated using the Fiji 'analyze particle' tool and the $ThioS^+$ area and circularity were calculated for each plaque. For quantification of the phagosome area and internalized plaques using CD68, Iba-1 and ThioS, the area above a set fluorescent threshold each for $CD68^+$, Iba-1^+ and $ThioS^+$ areas were calculated, and first $CD68^+$ Iba-1^+ double-positive areas were calculated using the Fiji 'image calculator' tool (with AND operation) and measured % $CD68^+$ Iba-1^+ areas as phagosome, and then the $CD68^+$ Iba-1^+ $ThioS^+$ area was calculated using the Fiji 'image calculator' tool (with AND operation) and measured % $CD68^+$ Iba-1^+ $ThioS^+$ areas as internalized plaques, and visualized as 3D reconstruction images using Imaris. For quantification of dystrophic neurites, the $LAMP1^+$ area was calculated above a set fluorescent threshold and summed using the Fiji 'analyze particle' tool and the ratio of summed area ($LAMP1^+$ area/$6E10^+$ area) was calculated per $6E10^+$ plaque. For quantification of $Clec7a^+$ area around $ThioS^+$ plaques, first defined plaque-associated area by 15 μm away from the edge of the nearest ThioS edge, area above set fluorescent thresholds for $Clec7a^+$ area was then measured using the Fiji 'measure' tool.

RNA isolation, cDNA synthesis, quantitative RT-PCR (qPCR)

Single cells were prepared from the left hemisphere of T2WT-AD and T2KO-AD mouse brains as described in the brain sample preparation section and stained with anti-CD45 (BioLegend; Cat# 103112; Clone 30-F11) and anti-CD11b (BioLegend; Cat# 101208; Clone M1/70) antibodies for 15–30 min at 4°C in the dark. After two washes with flow cytometry staining buffer, cells were resuspended in flow cytometry staining buffer with DAPI, and DAPI$^-$ CD45$^+$ CD11b$^+$ cells were directly sorted in 400 μL TRIzol LS (Life Technologies; Cat# 15596018) using a FACSAria II. Total RNA was extracted and then purified using a Qiagen RNeasy MinElute Cleanup Kit (Qiagen; Cat# 74204) according to the manufacturer's protocol. Quality and quantity of RNA was assessed on a Bioanalyzer (Agilent) at The Protein and Nucleic Acid (PAN) Biotechnology Facility of Stanford University, and samples with RNA integrity number over 8.0 were used for subsequent analysis. For quantitative PCR (qPCR), a total of 50 ng of total RNA was reverse transcribed using SuperScript III reverse transcriptase (Thermo Fisher Scientific; Cat# 18080044) to prepare cDNA. qPCR was performed by using SYBR Master Mix (Thermo Fisher Scientific; Cat# 4309155) and the Applied Biosystems QuantStudio 7 (Applied Biosystems). The following cycles were performed: an initial denaturation cycle of 94°C for 5 min, followed by 40 amplification cycles of 94°C for 15 s and 60°C for 1 min). The transcript levels were determined after normalization against *Gapdh* as described.[69] The primers (Table S2) were chosen from Primer Bank.[70]

Droplet digital PCR (ddPCR)

Brain- and PB samples were prepared as described in brain sample preparation and PB analysis. Genomic DNA (gDNA) was purified from cells using the Quick DNA miniprep kit (Zymo Research; Cat# D3024). gDNA was eluted in nuclease-free water. The concentration of gDNA was determined with a Nanodrop Spectrophotometer ND-1000 and adjusted to indicated concentrations with nuclease-free water. gDNA was used as a template for ddPCR, and ddPCR performed according to manufacturer's instructions for the BioRad QX200 system. Briefly, ddPCR reactions were prepared using 2x ddPCR supermix (BioRad; Cat# 1863025), biallelic reference-HEX primer/probe mix (IDT PrimeTime Std qPCR Assay: primer/probe ratio: 3.6, Primer 1: GGATGGGGAACGCAGCTCTT, Primer 2: AGTGCGGCAGAATACAGCA, probe:/5HEX/TGATGGGTT/ZEN/GTGAAGGCAGCTGCACCT/3IABkFQ/), and one of the following FAM-conjugated primer/probe mixes (all sourced from IDT as PrimeTime Std qPCR Assay; primer/probe ratio: 3.6): UTY-FAM (Primer 1: CTGTTAACATAAATATTGGTCCAG, Primer 2: CACAGAAGTCATTCAGAACAC, probe:/56-FAM/CTTCAGGTA/ZEN/CAACAAACCATTCACAATC/3IABkFQ/), or SRY-FAM (Primer 1: CCTACACAGAGAGAAATACCC, Primer 2: CAACTGCA GGCTGTAAAATGC, probe:/56-FAM/TCAGCCTCA/ZEN/TCGGAGGGCTAAAGTGTC/3IABkFQ/). After generation of droplets in the BioRad QX200 generator, which employed DG8 cartridges (BioRad; Cat# 1864008), gaskets (BioRad; Cat# 1863009), and droplet generation oil for probes (BioRad; Cat# 1863005), ddPCR mixes were loaded into 96 well plates (Fisher Scientific; Cat# E951020346) and sealed with pierceable foil heat seal (BioRad; Cat# 1814040). PCR reactions were run in a thermocycler using the following parameters: 1 × 10 min at 95°C, 41 × 30 s at 94°C followed by 1 min 5 s at 58°C (SRY & UTY assays), and 1 × 10 min at 98°C. Subsequently, ddPCR reactions were analyzed in a BioRad QX200 droplet reader and data analysis was performed with BioRad's QuantaSoftTM Analysis Pro 1.0 software. The percentage of male chimerism in female background was calculated via the following formula: ((concentration in copies per μL of SRY, or UTY-FAM signal*100)/concentration in copies per ul of biallelic reference-HEX signal) x 2 = % male. More than 10000 droplets were analyzed per sample.

RNA-sequencing analysis

Single cell suspension and total RNA were prepared from the mouse brain as described above. The SMART-Seq v4 Ultra Low Input RNA Kit (Takara Bio; Cat# 634890) was used to generate cDNA and libraries according to the manufacturer's protocol. The libraries were synthesized, indexed libraries were pooled and sequenced on NovaSeq platform (Illumina). 150 bp paired-end reads were generated producing a mean of 30.1 million reads per sample. RNA-sequencing data were processed and interpreted using in-house bioinformatic analysis pipelines in Sherlock computing clusters of The Stanford Research Computing Center. Briefly, raw sequencing reads were demultiplexed with bcl2fastq and aligned to mouse transcriptome (mm10; GRCm38.p6) using STAR (version 2.5.2b) with the default parameters. In summary, uniquely mapped reads were 77.75%; reads mapped to multiple loci 2.60%; reads mapped to too many loci 0.11%; reads unmapped (too short) 20.38%; reads unmapped (other) 0.16%. The expression of Gencode-annotated was calculated using HTSeq-count,[71] and FPKM/TPM values were calculated using RSEM with the default parameters.[72] Raw counts of each gene were normalized, and genes with low counts were removed using the mean of normalized counts as a filter statistic, performed principal component analysis, and conducted differential expression analysis using the DESeq2 package (3.17)[73] in R with standard parameters. The p values were corrected with the false discovery rate (FDR) procedure to limit false positives arising from multiple testing. Differentially expressed genes were selected by applying $P_{adj.}$ cutoffs less than 0.05 and log2 fold change of at least ±1. Heatmaps were generated using the 'pheatmap' or ggplot2 R packages. Functional enrichment analysis for gene ontology terms and pathway was performed using g:Profiler and visualized using ggplot2 R package.[74] Single-cell RNA-seq datasets of 7-month-old Trem2$^{-/-}$ 5xFAD mice brain were obtained from GSE140511 of Gene Expression Omnibus and proceed with default parameters described in previous study[41] using Seurat R package. Curated gene expression profiles of human AD patients (syn18485175; ROSMAP)[42] were obtained from The Myeloid Landscape 2, and the gene expression was visualized using ggplot2 R package.[75]

QUANTIFICATION AND STATISTICAL ANALYSIS

In this study, 'n' represents number of animals used in experiments. For quantification in brain sections, we used at least three sections per animal. The number of brain sections used for quantification is presented in the figure legends. All bar graphs are mean values ±SEM. Statistical comparisons between two groups were made using unpaired, two-tailed, Student's *t* test and were calculated using Prism software (GraphPad). Chi-square T value was calculated using FlowJo 'Compare Populations' function. p values less than 0.05 were considered significant.